

Landscape Predictions for the Higgs Boson and Top Quark Masses

Brian Feldstein, Lawrence J. Hall and Taizan Watari¹

*Department of Physics and Lawrence Berkeley National Laboratory,
University of California, Berkeley, CA 94720, USA*

Abstract

If the Standard Model is valid up to scales near the Planck mass, and if the cosmological constant and Higgs mass parameters scan on a landscape of vacua, it is well-known that the observed orders of magnitude of these quantities can be understood from environmental selection for large scale structure and atoms. If in addition the Higgs quartic coupling scans, with a probability distribution peaked at low values, environmental selection for a phase having a scale of electroweak symmetry breaking much less than the Planck scale leads to a most probable Higgs mass of 115 GeV. While fluctuations below this are negligible, the upward fluctuation is $25/p$ GeV, where p measures the strength of the peaking of the a priori distribution of the quartic coupling. There is an additional ± 6 GeV uncertainty from calculable higher loop effects, and also sensitivity to the experimental values of m_t and α_s . If the top Yukawa coupling also scans, the most probable top quark mass is predicted to lie in the range (172.4–176.9) GeV, providing the standard model is valid to at least 10^{17} GeV, with an additional uncertainty of ± 3 GeV from higher loops. The downward fluctuation is $35 \text{ GeV}/\sqrt{p}$, suggesting that p is sufficiently large to give a very precise Higgs mass prediction. While a high reheat temperature after inflation could raise the most probable value of the Higgs mass to 124 GeV, maintaining the successful top prediction suggests that reheating is limited to about 10^9 GeV, and that the most probable value of the Higgs mass remains at 115 GeV. If all Yukawa couplings scan, then the e, u, d and t masses are understood to be outliers having extreme values induced by the pressures of strong environmental selection, while the s, μ, c, b, τ Yukawa couplings span only two orders of magnitude, reflecting an a priori distribution peaked around 10^{-3} . An interesting extension to neutrino masses and leptogenesis follows if right-handed neutrino masses scan, with a preference for larger values, and if T_R and T_{\max} scan with mild distributions. The broad order of magnitude of the light neutrino masses and the baryon asymmetry are correctly predicted, while the right-handed neutrino masses, the reheat temperature and the maximum temperature are all predicted to be of order 10^9 GeV.

¹address after August '06: Caltech, Pasadena, CA 91125, USA

1 Introduction

The Standard Model (SM) of particle physics is both extremely successful and highly predictive. It has passed successive hurdles, from the discovery of weak neutral currents to the precision electroweak data from 10^7 Z decays. It even explains why protons are so stable and why neutrinos are so light. Despite these successes, it is generally not viewed as a fundamental theory, but as an effective field theory valid on scales less than about a TeV. This is because the Higgs boson mass parameter receives radiative corrections that are quadratically divergent, and therefore proportional to Λ_{SM}^2 , where Λ_{SM} is the maximum mass scale that the theory describes. For large values of Λ_{SM} , tree-level and radiative contributions to the Higgs mass parameter must cancel to a fractional precision of

$$\Delta \approx \left(\frac{0.5 \text{ TeV}}{\Lambda_{SM}} \right)^2 \left(\frac{m_H}{130 \text{ GeV}} \right)^2, \quad (1)$$

where m_H is the physical Higgs boson mass. For the SM to be valid up to 5 TeV, a cancellation by two orders of magnitude is already required, and to reach the Planck scale requires an adjustment finely tuned to 32 orders of magnitude. Theories that solve this naturalness problem, including technicolor, supersymmetry, composite Higgs bosons and extra spatial dimensions, have almost defined physics beyond the SM, and are the main focus of potential discoveries at the Large Hadron Collider.

Rather than just being a description of interactions beneath the TeV scale, if the SM is valid up to very large energies, for example to the Planck scale $M_{Pl} \simeq 2.4 \times 10^{18}$ GeV, then it predicts the mass of the Higgs boson to be in the range

$$115 \text{ GeV} < m_H < 180 \text{ GeV}. \quad (2)$$

The lower limit arises from stability of the SM vacuum [1, 2, 3, 4]. A light Higgs boson results in the quartic Higgs self interaction becoming negative at large energies; if it is too negative, then the universe undergoes quantum tunneling to a phase quite unlike the observed phase. On the other hand the upper bound results from perturbativity: if the Higgs mass is too heavy, the quartic self coupling becomes non-perturbative at scales well below the Planck scale. It is remarkable that the prediction (2) receives so little attention, since it closely coincides with the current experimental 95% C.L. range

$$114 \text{ GeV} < m_H < 175 \text{ GeV} \quad (3)$$

from direct searches and precision electroweak data, respectively [5]. For a natural SM with $\Lambda_{SM} \approx \text{TeV}$, the Higgs quartic coupling could lie in a range spanning two orders of magnitude, 0.03—3, whereas for a large value of Λ_{SM} the range is narrowed to a factor of 3, and consequently m_H is constrained to a factor of about $\sqrt{3}$.

If the LHC discovers physics beyond the SM, or if it discovers a heavy Higgs boson, then the apparent agreement between (2) and (3) will be seen to be a coincidence. However, if the LHC discovers a SM Higgs boson in the range of (2), and no physics beyond the SM, then the case for a very large Λ_{SM} will be considerably strengthened. In this case the LHC would have verified and extended the Little Hierarchy Problem already visible at LEP [6], and there would be two obvious interpretations: new physics could appear at several TeV and the SM could be accidentally unnatural with apparent fine-tunings at the percent level; alternatively the conventional understanding of naturalness could be completely wrong and Λ_{SM} could be extraordinarily large. The LHC would eventually yield a very precise measurement of the Higgs boson mass; could this discriminate between these two interpretations?

An alternative to naturalness is the idea that the universe contains many patches with differing underlying physics, and only those patches with a certain complexity will be the subject of observation. Thus certain observations can be explained from the selection of complexity rather than from symmetry principles [7]. If the weak scale is selected anthropically, i.e. by environmental requirements for complexity, the concept of naturalness is not needed to understand the hierarchy between weak and Planck scales [8]. In this picture, the fundamental theory of nature may contain a huge number of vacua, and the Higgs mass parameter may depend on the vacuum. If the universe contains many patches, each with its own vacuum, then essentially all possible values of the weak scale are realized somewhere in the universe. It is only in those patches where the weak scale is in the range of 100s of GeV that atomic physics provides the building blocks for carbon based life. The cut-off scale of the SM, Λ_{SM} , may be extraordinarily large, and the Higgs expectation value of most vacua may be of order of Λ_{SM} , yet such vacua are irrelevant to us, since we necessarily find ourselves in one of the very rare patches having hospitable chemistry.

Despite resistance from some physicists, these ideas—a landscape of vacua and environmental selection—have gained attention over the last decade: selection of patches of the universe containing large scale structures, such as galaxies, can essentially solve the cosmological constant problem and predicts that observers are likely to inhabit patches containing dark energy [9]. Furthermore, the number of known vacua of string theory continues to increase, and the string landscape appears to be able to scan parameters sufficiently densely to allow environ-

mental selection [10]. Such ideas should perhaps be resisted, since they are so difficult to test experimentally. How are we to test such theories when the other patches of the universe lie outside our horizon? Natural theories are tested by assuming a theory with a parameter space that is sufficiently restricted that predictions for observables can be made. In the landscape, predictions may be possible by combining environmental selection with assumptions about the underlying vacuum probability distributions. In this paper we argue that the Higgs boson mass is well suited to this sort of prediction, since it depends on the quartic scalar coupling, and if this coupling is too low the SM vacuum decays. If the landscape favors low values of this coupling, environmental selection will favor Higgs masses close to the stability bound.

Expanding the Higgs potential $V(\phi)$ in powers of ϕ/Λ_{SM} , the relevant part of the Higgs potential is

$$V(\phi) = \Lambda^4 + m^2\phi^\dagger\phi + \lambda(\phi^\dagger\phi)^2. \quad (4)$$

In this paper we assume that the entire SM Higgs potential varies, or scans, from one patch of the universe to another. The scanning of Λ^4 leads to the scanning of the cosmological constant and allows an environmental selection for galaxies, largely explaining the observed value of the dark energy [9]. Similarly, the scanning of the Higgs mass parameter m^2 and quartic coupling λ allows for the environmental selection of required atomic properties, determining the weak scale $\sqrt{-m^2/\lambda}$ [8]. In those regions of the universe selected environmentally by both the cosmological constant and the weak scale, there will be a variation in the coupling λ and therefore in the Higgs boson mass from one patch to another. What are the physical consequences of this scanning of the Higgs quartic coupling λ ? Environmental selection will choose the required electroweak phase: we must live in a region with λ above a minimum value, λ_c . This is how the usual stability limit on the SM Higgs boson mass arises in the landscape, leading to the lower bound in (2). For $\lambda > \lambda_c$ there is no obvious environmental selection of one value of m_H over another, hence the prediction for the Higgs boson mass is governed by the probability distribution² $P(\lambda)$ of the coupling λ in the vacua with acceptable large scale structure and atomic physics. To proceed, apparently one needs a calculation of $P(\lambda)$ from the landscape. In fact, only a single assumption on its form is required: we assume that $P(\lambda)$ is sufficiently peaked at low values that λ is expected to be near λ_c , as illustrated in Figure 1, corresponding to a Higgs mass near the stability bound. The precision of this prediction clearly depends on how steep $P(\lambda)$ is near λ_c , as we investigate in some detail.

It is important to stress that our prediction does depend on an assumption for $P(\lambda)$. For

²To be more precise, by the probability distribution $P(m^2, \lambda)|_{\sqrt{-m^2/\lambda}=174 \text{ GeV}}$. Hereafter, we mean this by $P(\lambda)$.

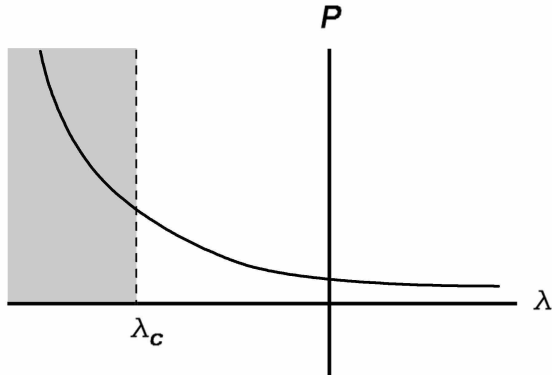


Figure 1: The a priori probability distribution is peaked at low values of λ .

example, an alternative assumption that $P(\lambda)$ is peaked at large positive values of λ predicts m_H near the perturbativity limit of 180 GeV. However, this prediction could depend on whether the theory has a large energy interval in which it is strongly coupled before a perturbative quartic emerges at low energy. Furthermore, an observation of a Higgs boson mass in this region could be interpreted in terms of a strongly coupled fundamental theory without any recourse to the landscape. In the rest of this paper, we concentrate on the possibility that the probability distribution $P(\lambda)$ is peaked towards low values, corresponding to a Higgs boson mass near the stability limit of $m_H \approx 115$ GeV. A measurement of such a Higgs mass, together with the absence of any new physics, would provide evidence for environmental selection.

The top quark Yukawa coupling, h , plays an essential role in electroweak symmetry breaking in the SM with large Λ_{SM} , through its effect on the renormalization group (RG) scaling of the Higgs quartic coupling, λ . Suppose that h also scans in the landscape, so that there is a combined probability distribution $P(\lambda, h)$. How is the discussion of the Higgs mass prediction changed? As we will show, the metastability boundary in the (λ, h) plane has a special point, where λ is at a minimum, and a simple assumption for the a priori probability distribution, $P(\lambda, h)$, implies that patches of the universe in the desired electroweak phase are most likely to be in the neighborhood of this point. Remarkably, at this special point

$$m_{H_c} = (121 \pm 6) \text{ GeV} \qquad m_{t_c} = (175 \pm 2) \text{ GeV}, \qquad (5)$$

where the uncertainty corresponds to $\Lambda_{SM} = 10^{18 \pm 1}$ GeV, leading simultaneously to a prediction for the Higgs mass and to a successful post-diction for the top mass. Although there are further

uncertainties of about ± 6 GeV and ± 3 GeV on m_{H_c} and m_{t_c} respectively, from higher loop effects, this result is nevertheless very striking.³

It is well-known that the stability limit on m_H in the SM depends on T_R , the reheat temperature of the universe after inflation. In the landscape, T_R may scan from one patch of the universe to another, or it might be fixed; either way, we study the landscape Higgs mass prediction in two cases. In the first case, in sections 2 and 3, we assume that the probability distribution is dominated by patches having $T_R \lesssim 10^8\text{--}10^9$ GeV, so that thermal fluctuations can be ignored, and the stability limit arises from quantum fluctuations from the false vacuum. In section 2 we keep the top Yukawa coupling fixed, while in section 3 we allow it to scan. In the second case, in section 4, we assume that the landscape probability distribution is dominated by patches having $T_R \gtrsim 10^8\text{--}10^9$ GeV, and study the Higgs mass prediction arising from thermal nucleation of bubbles of the true vacuum. In section 5 we embed these ideas in the “scanning SM” where all SM parameters scan, discussing charged fermion mass hierarchies, the scale of neutrino masses, leptogenesis and consequences for inflation. Conclusions are presented in section 6.

2 Higgs Mass Prediction from Quantum Tunneling

2.1 Quantum Tunneling

In this section we predict the Higgs boson mass using the environmental constraint of sufficient stability of the electroweak vacuum in a landscape scenario. The SM is assumed to be valid up to a high energy scale, Λ_{SM} , such as the Planck scale. To be precise, we define Λ_{SM} to be the scale at which the standard model RG equations and bounce action calculations are still valid to within 1%. Thus Λ_{SM} is slightly lower than the scale at which new physics actually arises. We concentrate on the consequences of scanning $(\Lambda^4, m^2, \lambda)$, assuming that all other parameters of the SM do not effectively scan or are fixed tightly to observed values by other environmental constraints. In the patches of the universe dominating the probability distribution, the maximum temperature after inflation is assumed to be sufficiently low ($T_R \lesssim 10^8\text{--}10^9$ GeV) that thermal nucleation of the phase transition is sub-dominant.

At large field values, the effective potential of the Higgs field $H = \sqrt{2} \text{Re}(\phi^0)$ is well approx-

³We should mention here that predictions for the Higgs and top masses in the SM, assumed valid to very high scales, have been made based on very different principles. One prediction resulted from assuming that there are two degenerate electroweak vacua, with one occurring near the Planck scale [11], while another resulted from the assumption that two phases should coexist, giving borderline vacuum metastability [12].

imated by

$$V(H) = \frac{\lambda(H)}{4}H^4 \quad \text{for } H \gg v \equiv 246 \text{ GeV}, \quad (6)$$

where $\lambda(H)$ is the value of the running Higgs quartic coupling evaluated at the scale $\mu = H$. The RG equation for λ has the 1-loop form

$$16\pi^2 \frac{d\lambda}{d\ln\mu} = 24\lambda^2 + 12\lambda h^2 - 6h^4 - 9\lambda g_L^2 - 3\lambda g_Y^2 + \frac{3}{8}g_Y^4 + \frac{3}{4}g_L^2 g_Y^2 + \frac{9}{8}g_L^4, \quad (7)$$

where h is the top Yukawa coupling, and g_L and g_Y are the $SU(2)_L$ and $U(1)_Y$ gauge couplings, respectively. Several trajectories for $\lambda(\mu)$ are illustrated in Figure 2. The effect of the large top Yukawa coupling is to reduce the value of λ at high energies. In fact, λ will become negative below Λ_{SM} if its value at $\mu \approx v$ is too small. In such cases, the minimum with $\langle H \rangle = v$ is not the true minimum of the potential, and we must consider the possibility of the universe tunneling quantum mechanically from our hospitable $\langle H \rangle = v$ vacuum to the inhospitable one with very large $\langle H \rangle$.⁴ Throughout we assume that conditions of the early universe lead to a sufficient number of patches with the desired metastable phase.

The quantum tunneling rate per unit volume to the true vacuum is dominated by a bounce solution $H(r)$. A pure up-side-down quartic potential, (6) with negative λ , has an SO(4) symmetric bounce solution [13]. Due to the conformal nature of the potential (ignoring the running of λ and the quadratic term of order the weak scale), there is a family of bounce solutions, $H(r) = cH_0(cr)$ for $c > 0$, with different size $\propto 1/c$ and field value at the center $H(r=0) \propto c$. A bounce solution with $H(r=0) = M$ contributes to the decay rate an amount

$$\Gamma(M) \approx M^4 e^{-\frac{8\pi^2}{3|\lambda(M)|}}, \quad (8)$$

so that the total decay rate is approximated by [1, 2, 3, 4]

$$\Gamma[\lambda_0] \approx \max_{M < \Lambda_{SM}} \Gamma(M) = \max_{M < \Lambda_{SM}} \left[M^4 e^{-\frac{8\pi^2}{3|\lambda(M)|}} \right]. \quad (9)$$

Each patch of the universe has its own $\lambda_0 \equiv \lambda(\Lambda_{SM})$, RG trajectory $\lambda(\mu)$, and corresponding decay rate $\Gamma[\lambda_0]$. By time t , an arbitrary point remains in the desired false vacuum with $\langle H \rangle = v$ provided no bubble nucleated in its past light cone. Since the vacuum tunneling rate $\Gamma[\lambda_0]$ does not depend on time, bubble nucleation is most likely to occur at the epoch with time of order t , rather than at a much earlier epoch. Assuming that the universe has been matter

⁴In this phase the ratio of quark masses to the QCD scale and to the Planck mass are very far from allowing conventional nuclei and cosmology.

dominated most of the time until t , the fraction of the volume of a patch in the false vacuum at time t is given by [14]

$$f(\lambda_0; t) = e^{-\Gamma[\lambda_0]t^4}, \quad (10)$$

where a coefficient of order one in the exponent is ignored.^{5,6}

For practical applications, we are interested in t of order 10^{10} years; t is either still in the matter-dominated era or in the dark-energy dominated era so that the exponent is roughly of order $\Gamma[\lambda_0]\tau^4$, where $\tau = 10^{10}$ years. If $\Gamma(M)\tau^4 \gtrsim 1$ for any scale in the range $v \ll M \lesssim \Lambda_{SM}$, the survival fraction $f(\lambda_0; \tau)$ is significantly less than 1. Since $\Gamma(M)$ primarily depends on $\lambda(\mu)$ renormalized at $\mu = M$, one can introduce a critical value of the quartic coupling $\lambda_c(M)$ by $\Gamma(M)\tau^4 \simeq 1$

$$\lambda_c(M) \simeq -\frac{2\pi^2}{3} \left(\frac{1}{\ln(M_{Pl}\tau) + \ln \frac{M}{M_{Pl}}} \right) \approx -0.047 \left(1 + \frac{1}{138} \ln \frac{M_{Pl}}{M} \right), \quad (11)$$

where $\ln(M_{Pl}\tau) \approx 138$ is used to obtain the last expression. This critical line of stability, $\lambda_c(M)$, is shown by a dashed line in Figure 2. Whenever a trajectory $\lambda(\mu)$ dips below $\lambda_c(\mu)$ at any scale $v \ll \mu \lesssim \Lambda_{SM}$, bounces with $H(r=0)$ of order that scale would have destabilized the desired false vacuum. The usual metastability bound on the Higgs boson mass in [2, 3, 4] corresponds to the trajectory that touches the critical line of stability at one scale $\mu = M_{dom} \sim 10^{17}$ GeV, while maintaining $\lambda(\mu) \geq \lambda_c(\mu)$ for all μ up to Λ_{SM} . Thus, the bounce of most danger is the one with $H(r=0) = M_{dom}$, and the metastability bound is independent of Λ_{SM} provided $\Lambda_{SM} > M_{dom}$. Note that there is an assumption here: for all trajectories of interest, the contribution to $\Gamma[\lambda_0]$ from quantum fluctuations to field values larger than Λ_{SM} are sub-dominant. We must assume this because we cannot calculate these contributions without knowing some of the details of the more complete theory above Λ_{SM} . The trajectories of interest include the special one, shown as a solid curve in Figure 2, and all those that lie above it. The assumption is reasonable because, as the SM begins to break down at energies just above Λ_{SM} , these trajectories all lie above the critical curve $\lambda_c(\mu)$, shown dashed in Figure 2.

A landscape will provide some a priori probability $P(\lambda_0)$, and we follow the principle that the probability distribution of observable parameters is further weighted by the fraction of

⁵The exponent depends non-perturbatively on the Higgs quartic coupling λ as in (8), and, if $|\lambda|$ is small, a small variation in the value of λ can change Γ by orders of magnitude. Thus, any prefactor of order unity to Γt^4 is unimportant compared with the sensitivity on λ .

⁶As the universe evolves into an era dominated by the cosmological constant the fraction of the volume in the false vacuum is given asymptotically by $f(\lambda_0; t) = e^{-\Gamma[\lambda_0]t/H_0^3}$, where H_0 is the Hubble parameter and a coefficient of order one in the exponent is again ignored.

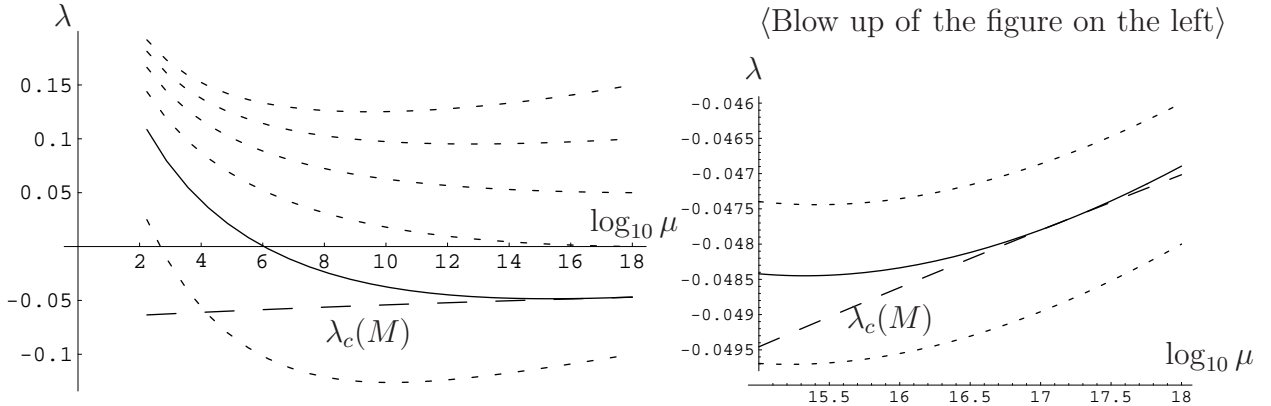


Figure 2: Several RG trajectories for the Higgs quartic coupling, λ , are shown by dotted curves. The dashed line gives the critical coupling λ_c at each energy, defined by (11). The special trajectory that corresponds to the usual SM metastability bound is shown by a solid curve. Any patch of the universe with a trajectory that passes significantly into the region below the dashed line is likely to decay out of the false vacuum with $\langle H \rangle = v$ before a cosmological time scale of order 10^{10} years. In this figure, Λ_{SM} is chosen to be 10^{18} GeV, and $(g_Y, g_L, g_s, h)|_{\mu=\Lambda_{SM}} = (0.466, 0.512, 0.500, 0.407)$ yielding, for the special trajectory with $\lambda_0(\Lambda_{SM}) = -0.0469$, weak-scale SM parameters $(\alpha(m_Z)^{-1}, \sin^2 \hat{\theta}_W(m_Z), \alpha_s(m_Z), m_t) = (127.9, 0.2313, 0.1176, 172.5 \text{ GeV})$ [15] as well as $m_H = 115$ GeV. The analysis is performed with 2-loop RG equations [16] and 1-loop (2-loop in g_s) threshold corrections [17, 18, 19] at the matching scale $\mu = m_t$ [20].

observers who see them. For patches of the universe having $\lambda(\Lambda_{SM}) = \lambda_0$, only a volume fraction $f(\lambda_0; t)$ remains in our desired false vacuum with $\langle H \rangle = v$, introducing an additional λ_0 dependence in the total probability distribution

$$\mathcal{P}(\lambda_0; t) d\lambda_0 = P(\lambda_0) e^{-\Gamma[\lambda_0] t^4} d\lambda_0. \quad (12)$$

The a priori distribution $P(\lambda_0)$ describes all λ_0 dependence that originates from cosmology up to the end of (the last) inflation. Since the Higgs boson mass itself is not environmentally important, f will be the only λ_0 dependence (and Higgs boson mass dependence) that originates after the end of inflation.

One could also study an all-time probability distribution, instead of the distribution for contemporary observers. Such a distribution is obtained by integrating (12) over t , weighted by the time evolution of the number of observers, $\rho(t)$, which we expect to be independent of λ_0 . Thus, f still remains the only source of the late-time dependence of the distribution on the Higgs boson mass.

2.2 The Prediction

Using the probability distribution of (12) we would like to answer three key questions.

1. What is the most probable value of λ_0 , and therefore the Higgs mass, as seen by observers, such as us, living at the present age of the universe $t = t_0 \sim 1.4 \times 10^{10}$ years?
2. What range of Higgs masses correspond to a probability within a factor of, say, $1/e$ of the peak probability?
3. What fraction of observers in the “multiverse” live at the time t_0 or later?

The answer to the first question gives the central value of the Higgs mass prediction, while the answer to the second gives a measure of the uncertainty of the prediction. We will be particularly interested in how these two answers depend on the form of the a priori probability distribution $P(\lambda_0)$. We suspect that a precise prediction will follow only if there is some peaking in this distribution. There may be a trade-off: if the distribution is too weak, then we cannot predict the Higgs mass with significant accuracy; if it is too strong, then we may find ourselves living in an unstable patch of the universe that was extremely lucky to survive until now. With the third question, we thus investigate how much peaking we can tolerate before observers living as late as t_0 become a rarity.

We assume that $\Lambda_{SM} \gtrsim M_{dom}$. Since tunneling is most likely to occur at the scale M_{dom} , as can be seen from figure 2, with this assumption the analysis becomes independent of Λ_{SM} . Consider patches of the universe with various values of $\lambda(M_{dom})$ as illustrated by the trajectories in Figure 2. An a priori probability distribution peaked at low values of λ_0 , as illustrated in Figure 1, means that there are more patches with $\lambda(M_{dom})$ below the critical value $\lambda_c(M_{dom})$ than above. However, these patches are more likely to decay. The most probable observed value of λ today is therefore determined by a competition between $P(\lambda_0)$ and $e^{-\Gamma t_0^4}$ in (12), and is given by⁷

$$\bar{\lambda}(M_{dom}) = \lambda_c(M_{dom}) \left(1 - \frac{1}{553} \ln \frac{553}{p} \right) \quad (13)$$

where the parameter p describes the strength of the peaking of the a priori probability distribution at $\lambda_0 = \lambda_c(\Lambda_{SM}) \equiv \lambda_{c,0}$ and is defined by

$$p = \left. \frac{\partial \ln P(\lambda_0)}{\partial \ln \lambda_0} \right|_{\lambda_0 = \lambda_{c,0}}. \quad (14)$$

⁷We ignore the difference between t_0 and $\tau = 10^{10}$ years, and use the latter as a reference. \bar{m}_H in (15) increases no more than 0.1 GeV by using t_0^4 instead (e.g., [4]).

Since λ_c is negative, we are interested in positive values for p . (Note that we use $\lambda_{0,c}$ and $\lambda_{c,0}$ interchangeably.) Clearly, except for extremely large values of p , the double exponential form of the decay probability factor is so powerful that we can just take $\bar{\lambda}(M_{dom}) = \lambda_c(M_{dom})$. Thus the most probable Higgs mass measured by observers at time t_0 corresponds to the solid line trajectory in Figure 2, which also corresponds to the usual SM metastability bound. We find that this trajectory corresponds to a Higgs boson mass⁸

$$\bar{m}_H = 115 \text{ GeV} + 6 \text{ GeV} \left(\frac{m_t - 172.5 \text{ GeV}}{2 \text{ GeV}} \right) - 2.6 \text{ GeV} \left(\frac{\alpha_s - 0.1176}{0.002} \right) \pm 6 \text{ GeV}. \quad (15)$$

There are several theoretical uncertainties that contribute to the ± 6 GeV uncertainty quoted in (15), in particular in relating the physical Higgs boson mass to the running quartic coupling evaluated at very high energies and in relating the physical top quark mass to the running top quark Yukawa coupling. It is perhaps fortunate that the TeVatron Run 2 data has lowered the top quark mass by about 2 GeV, since this implies that there is a smaller allowed range of the Higgs boson mass that could be interpreted as a successful prediction from the landscape. The present 7 GeV uncertainty in \bar{m}_H coming from the ± 2.3 GeV experimental uncertainty in m_t will be reduced by a factor of 2–4 at the LHC, depending on how well systematic uncertainties can be understood, while a reduction in the uncertainty in α_s may have to wait for the ILC. Finally, while \bar{m}_H is the most probable value for us to observe, a crucial question is the width of the probability distribution for the Higgs mass, which will depend on the strength p of the peaking of the a priori distribution $P(\lambda_0)$.

Reference [21] has studied extensions of the SM where m^2 scans but not λ . It was assumed that λ_0 is negative so that the RG trajectory for λ passes through zero at some scale Λ_{cross} . Only those patches of the universe with m^2 negative and $|m^2| < \Lambda_{cross}^2$ will have a metastable hospitable electroweak phase, and hence environmental selection will lead to the weak scale being close to Λ_{cross} , giving an alternative understanding of a low weak scale. This is a very interesting idea, but we stress that it is very different from the scanning of λ that this paper is based on. From Figure 2 it is clear that their idea cannot work in the SM, hence in addition to a light Higgs boson, they predict other heavy states at the weak scale.

2.3 The Width of the Prediction

If the SM is valid to very high energy scales, then the Higgs mass must lie in the range of (114–175) GeV. To see evidence for a landscape, it is crucial that the probability distribution

⁸Our result is 5 GeV higher than the metastability bound found in [4]; the 1-loop functional determinant contribution $\Delta S \sim -10$ [4] accounts for less than 1 GeV.

for the Higgs boson mass is sharply peaked compared to this allowed range. How strong an assumption does this require for the a priori probability distribution?

To study this question we Taylor expand the probability $\mathcal{P}(\lambda_0) \propto P e^{-\Gamma\tau^4}$ of (12) about the most probable value of the quartic coupling $\bar{\lambda}_0$, and find the couplings λ_{\pm} where \mathcal{P} falls to $1/e$ of its maximum value. We choose $\lambda_- < \lambda_+$, so that λ_+ corresponds to the heaviest Higgs boson that we are likely to observe. The maximum value of the exponent $\bar{\Gamma}\tau^4$ is $p/550$, which, for reasons discussed in the next sub-section, we take to be less than unity. It follows that the curve $\mathcal{P}(\lambda_0)$ is highly asymmetrical about $\bar{\lambda}_0$, with λ_- determined by the very rapid drop off of $e^{-\Gamma\tau^4}$

$$\lambda_- = \bar{\lambda}_0 \left(1 + \frac{1}{550} \ln \frac{550}{p} \right), \quad (16)$$

and λ_+ determined⁹ by the drop off of P

$$\lambda_+ = \bar{\lambda}_0 \left(1 - \frac{1}{p} \right). \quad (17)$$

We immediately see that, to obtain a significant Higgs mass prediction, there is no need to have a very large p ; a much more modestly peaked a priori distribution is sufficient. We also see that for modest values of p , the uncertainty in the Higgs mass coming from the landscape, i.e. from the unknown a priori probability distribution and from the probabilistic nature of quantum tunneling, is dominated by the $1/p$ contribution to λ_+ , which *increases* the Higgs boson mass above \bar{m}_H . The difference between λ_- and $\bar{\lambda}_0$ corresponds to a change in the Higgs mass that is negligible compared to the uncertainties of (15). Hence, while \bar{m}_H of (15) is the most probable value for the Higgs mass, the expected range is from \bar{m}_H up to $\bar{m}_H + \Delta m_H$ where Δm_H is determined from the shift in the quartic coupling at Λ_{SM} : $\Delta\lambda \approx |\lambda_{0,c}|/p \approx -.05/p$. RG running will not change this shift by much as it is taken to the weak scale, and since $m_H \sim 350\sqrt{\lambda}$ GeV, we find¹⁰

$$\Delta m_H \approx \frac{25 \text{ GeV}}{p}. \quad (18)$$

A very precise prediction follows if $p \geq 10$, while a reasonably precise prediction requires only $p \geq 3$. In the more complete theory at the scale of new physics, the description of the relevant landscape of vacua may involve a probability distribution with some other set of couplings.

⁹We caution the reader that on Taylor expanding P about $\bar{\lambda}_0$, the expansion is on the verge of breaking down on reaching λ_+ . We have checked that (17) is precisely accurate for the cases of power law and exponential distributions, but in general it should only be taken at the factor of 2 level.

¹⁰A different expression is required for $p \gtrsim \mathcal{O}(500)$, but for such large values, the predicted range is so narrow that the precise width is unimportant.

The simple peaking of P , corresponding to $p \geq 3$, may have a simple origin in the distributions of the more complete theory, because such a peaking is not destroyed by mild RG scaling.

2.4 The Fraction of Observers Living After t_0

There is a second important consequence of having the a priori probability distribution strongly peaked at low values of λ_0 : it becomes more probable for observers in the multiverse to live soon after non-linearities in the large scale structure appear. Once again, this can be understood by studying figure 2. As lower values of λ_0 become more strongly preferred, so more patches of the multiverse have $\lambda(M_{dom}) < \lambda_c(M_{dom})$, and these patches typically decay before time t_0 . This is clearly a problem if there are so few patches of the universe that survive until t_0 , that we are very rare observers. How does this limit the degree of peaking of $P(\lambda_0)$?

To get a feel for this we can study how P varies as λ_0 is decreased below λ_c . Instead of using λ_0 as the variable describing each patch we can use t , the time at which the patch with coupling λ_0 typically decays. Taylor expanding about t_0 to first order, we find

$$P(t) = P(t_0) \left(1 + \frac{p}{140} \ln \frac{t_0}{t} \right). \quad (19)$$

The earliest relevant time is the time that suitable structures first went non-linear, t_{NL} , and we expect that $\ln(t_0/t_{NL})$ is no more than a few. Hence we see that observers at t_0 are common in the multiverse providing the peaking of the probability distribution satisfies

$$p \leq \frac{140}{\ln(t_0/t_{NL})}, \quad (20)$$

which certainly allows for a precise Higgs mass prediction, as can be seen from (18).

Even for larger values of p the probability for observers in the multiverse at time t_0 does not drop extremely quickly. Approximating the time evolution of the number of observers in an undecayed patch, $\rho(t)$, as a step function at t_{NL} , the fraction of observers in the multiverse living at time t_0 or later is

$$f = \frac{I(t_0)}{I(t_{NL})} \quad (21)$$

where

$$I(t) = \int_t^\infty P(\lambda_0) e^{-\Gamma[\lambda_0]t'^4} dt' d\lambda_0. \quad (22)$$

To evaluate this expression an explicit form for P is required. For example, for an exponential distribution

$$P = C e^{p \frac{\lambda_0}{\lambda_c}} \quad (23)$$

we find

$$f \approx \left(\frac{t_{NL}}{t_0} \right)^{\frac{p}{140}}, \quad (24)$$

so that the fraction of observers at t_0 is not highly suppressed even for p as large as several hundred. For a power law distribution, the times t in (24) are replaced with $\ln \Lambda_{SM} t$, allowing considerably larger values of p . To summarize: there is a wide range of p that gives a precise Higgs mass prediction while allowing observers at t_0 to be common.

3 Scanning the Top Quark Yukawa Coupling

In the previous section we made an important assumption: the only SM parameters scanning in the landscape were those in the Higgs potential. Of all the other SM parameters, the one in our patch of the universe that has the most importance for electroweak symmetry breaking is the top quark Yukawa coupling, h , via the RG equation for the scalar quartic coupling (7). Hence we now discuss the consequences of allowing h to scan, leaving a discussion of allowing other Yukawa couplings to scan until section 5.

Remarkably, we will show in this section that, allowing h to scan, we can go further than merely preserving the Higgs mass prediction of section 2; using a landscape probability distribution, $P(\lambda_0, h_0)$, peaked in λ_0 beyond the SM metastability boundary, we will be able to add a successful understanding of the top quark mass to our prediction for the Higgs mass.

In this section we again assume that the temperature was never above about 10^8 – 10^9 GeV, at least for the patches of interest that dominate the probability distribution and evolved to the desired metastable phase, so that we may ignore effects of vacuum transition by thermal excitation.

3.1 The Metastability Boundary in the λ – h Plane

When only λ_0 scans, the metastability boundary is given by the critical value of λ_0 that corresponds to $\lambda(M_{dom}) = \lambda_c(M_{dom})$. If λ_0 and h_0 both scan, what is the critical line for the metastability boundary in the λ_0 – h_0 plane? As noted in the introduction, it has a special shape that will make an understanding of the top quark mass possible.

Consider a scale $\Lambda \leq \Lambda_{SM}$, and fix a value of $\lambda(\Lambda)$. Figure 3a shows trajectories of λ , starting from this initial condition, for various values of h . In the figure, $\Lambda = M_{dom}$ was used, but the qualitative picture is independent of this choice. When the top Yukawa is too small or too large, λ runs into the forbidden unstable region. As $\lambda(\Lambda)$ becomes smaller, the allowed

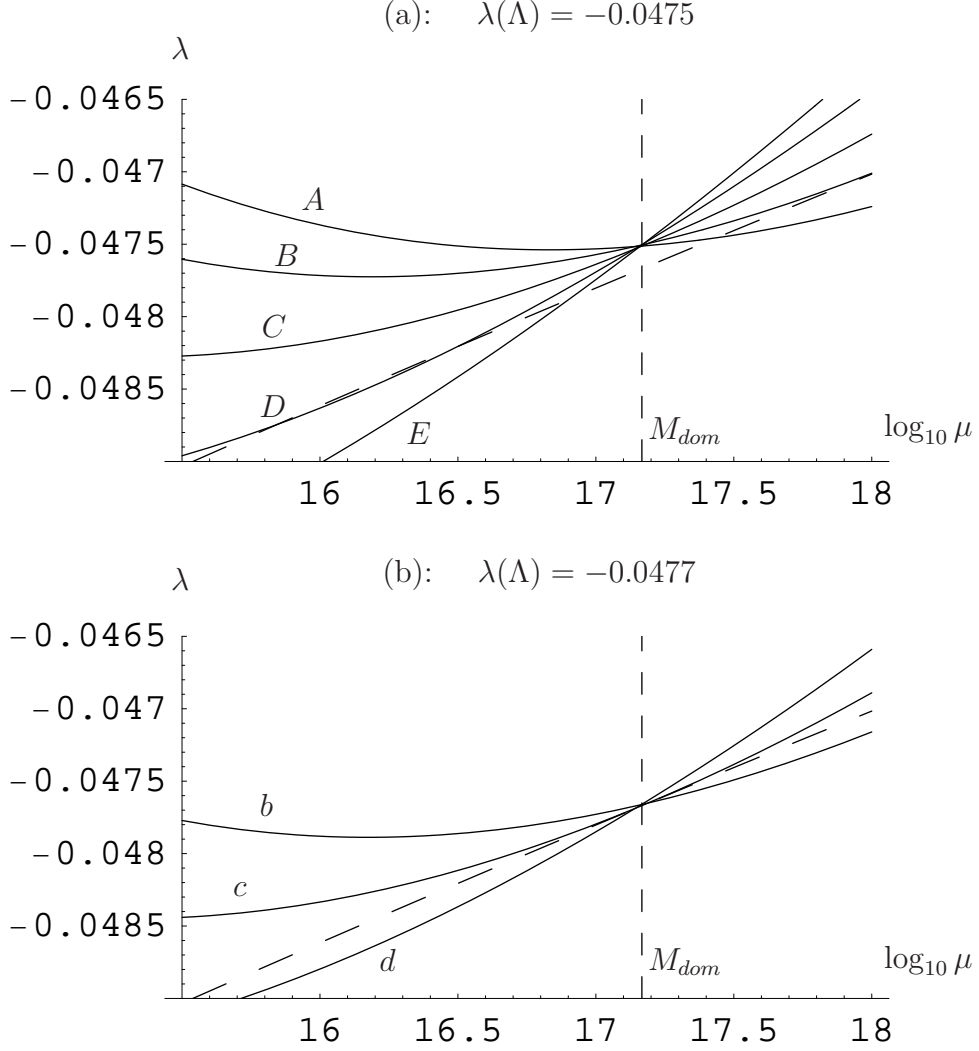


Figure 3: RG trajectories for $\lambda(\mu)$, for different values of h and a fixed value for $\lambda(\Lambda)$, shown for a few decades in energy below $\Lambda_{SM} = 10^{18}$ GeV. The scale Λ is chosen to be 1.5×10^{17} GeV, corresponding to the value of M_{dom} found in section 2 for the special trajectory with $\lambda_0(\Lambda_{SM}) = -0.0469$ that gives $m_t = 172.5$ GeV and $m_H = 115$ GeV. The trajectories in the upper panel labeled A, B, C, D and E have $\lambda(\Lambda) = -0.0475$ with $h(\Lambda) = 0.436, 0.429, 0.417, 0.406$ and 0.396 , respectively. Those in the lower panel, labeled b, c and d , are for $\lambda(\Lambda) = \lambda_c(\Lambda) = -0.0477$, with $h(\Lambda) = 0.429, 0.417$ and 0.406 . In both panels the dashed line is the line of metastability. The analysis uses SM RG equations at the 2-loop level. The gauge couplings at Λ_{SM} are not scanned, but are fixed to the values $(g_Y, g_L, g_s)(\Lambda_{SM}) = (0.466, 0.512, 0.500)$ for all trajectories, the same as in Figure 2. Uncertainties from higher loops and from the experimental uncertainty on α_s are not included.

range of h shrinks accordingly. When $\lambda(\Lambda)$ actually lies on the metastability boundary itself, as in Figure 3b, the only permissible value of h remaining is the one for which λ runs parallel to the boundary at the chosen scale, trajectory c of Figure 3b. The resulting metastability boundary in the $\lambda(\Lambda)$ – $h(\Lambda)$ plane is shown in Figure 4a. The trajectories labeled A, B, C, D, E and b, c, d in Figure 3 appear as points in Figure 4. The special trajectory c in Figure 3b is clearly at a special location on the metastability boundary in Figure 4a. If there is a probability pressure in the landscape pushing $\lambda(\Lambda)$ towards $\lambda_c(\Lambda)$, as in section 2, then we may simultaneously obtain the prediction that $h(\Lambda)$ will lie at the critical value corresponding to the trajectory c .

Now, the low energy value of the top mass corresponding to the critical point depends on the actual scale Λ we choose. If Λ is increased, the general shape of the metastability boundary remains the same, as shown in Figure 4b for $\Lambda = 10^{18}$ GeV, but the special trajectory has changed from c to near B , with a consequent change in the top mass prediction. The prediction for h should be made at the scale at which there is peaking in the probability distribution pushing towards the critical point. Although with h scanning, this is not a RG invariant requirement, it is a reasonable possibility for this to occur close to the scale of new physics, in particular, at the SM cutoff Λ_{SM} . What is remarkable is that if we take $\Lambda = \Lambda_{SM}$ to be within a few orders of magnitude of the Planck scale, then the corresponding prediction for h yields a value for the top mass that agrees closely with experiment. The uncertainty from varying $\Lambda = \Lambda_{SM}$ is mild.

The astute reader will notice a problem with this analysis; the λ – h metastability boundary was derived using the SM RG equations and tunneling rate calculations, which are expected to break down above the scale Λ_{SM} . As a result of effects from the new physics, the λ_0 – h_0 metastability boundary will differ from the form shown in Figure 4, and is sketched in Figure 5. However, the possible deviations are greatly restricted: only the half of the curve to the right of the critical point, corresponding to tunneling events to scales beyond Λ_{SM} , will be affected. Moreover, this part of the curve cannot change in an arbitrary way; $\lambda_{0,c}$ is still a strict lower bound on the Higgs quartic at Λ_{SM} , and thus the true curve must lie above the dashed line of Figure 5. As long as the true curve rises somewhat above this horizontal line, the central value of our prediction will be unchanged. If this curve did remain too flat, however, our prediction would have a large error bar on the high side; m_t would have a lower bound, but not much of an upper bound. This situation could arise if tunneling events to scales larger than Λ_{SM} are very suppressed.¹¹ To obtain a well controlled prediction for m_t , we will thus make one additional

¹¹The tunneling rate depends exponentially on the action. The reason that the metastability boundary changes so gradually in the SM is because of tree-level scale independence. However, the tunneling rate of the

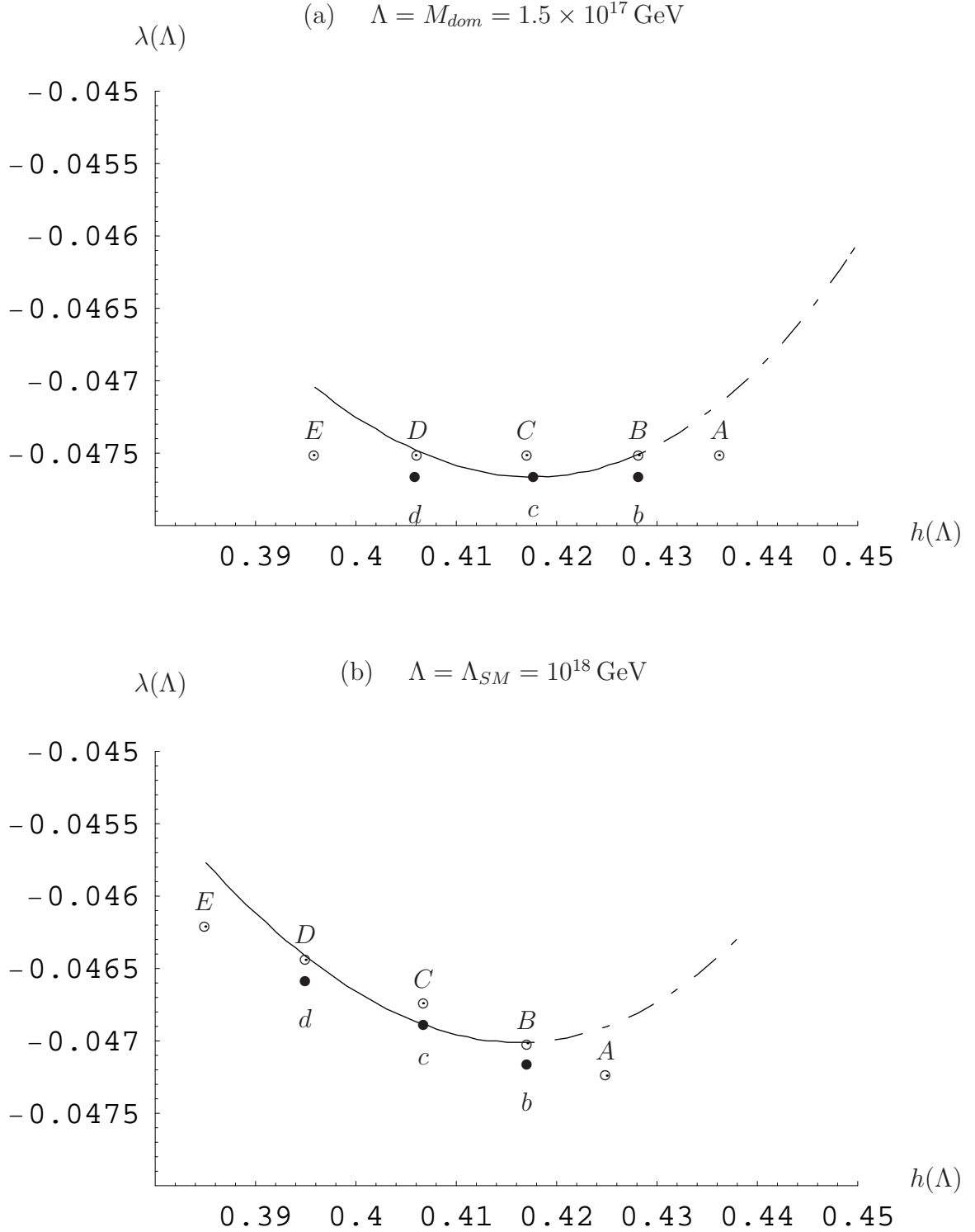


Figure 4: The metastability boundary in the $\lambda(\Lambda)$ – $h(\Lambda)$ plane for (a) $\Lambda = M_{dom}$, found for the metastability trajectory of section 2, and (b) $\Lambda = \Lambda_{SM} = 10^{18}$ GeV. The points labeled A, B, C, D, E and b, c, d correspond to the trajectories of Figure 3. The metastability boundary is shown dashed in regions where the calculation is unreliable; using SM equations, the dominant scale for tunneling is found to be above $\Lambda_{SM} = 10^{18}$ GeV.

assumption in this section: either

1. The metastability boundary rises sufficiently rapidly above $h_{0,c}$ so as to provide a reasonably sharp upper bound on the top mass, or
2. There is a fundamental probability distribution pressure in the landscape pushing h_0 towards smaller values, and hence towards $h_{0,c}$. We take $q = -\frac{\partial \ln P(\lambda_0, h_0)}{\partial \ln h_0} \Big|_c$, and require $1 \lesssim q \leq p$.

3.2 The Critical Value of the Top Mass

The critical value of the quartic coupling at any scale μ , $\lambda_c(\mu)$, is defined by $\Gamma(\mu)\tau^4 = 1$, where $\tau = 10^{10}$ years. By taking a derivative with respect to μ and using (8), we obtain

$$16\pi^2 \frac{d\lambda_c}{d \ln \mu} = 24\lambda_c^2. \quad (25)$$

On the other hand, the critical RG trajectory for λ , with h scanning, touches the curve $\lambda_c(\mu)$ tangentially at Λ_{SM} . In this way, the condition for the critical top Yukawa coupling h_c follows from

$$\left. \frac{d\lambda}{d \ln \mu} \right|_{\lambda_0=\lambda_{0,c}, \mu=\Lambda_{SM}} = \left. \frac{d\lambda_c}{d \ln \mu} \right|_{\mu=\Lambda_{SM}}, \quad (26)$$

giving

$$\left(12\lambda_c h_c^2 - 6h_c^4 - 9\lambda_c g_L^2 - 3\lambda_c g_Y^2 + \frac{3}{8}g_Y^4 + \frac{3}{4}g_L^2 g_Y^2 + \frac{9}{8}g_L^4 \right)_{\Lambda_{SM}} = 0. \quad (27)$$

Since $\lambda_{c,0} < 0$, the first 2 terms in (27) are negative while all the rest are positive. Taking $\lambda_{c,0}$ from equation (11), and using two loop SM RG running for $g_L(\Lambda_{SM})$ and $g_Y(\Lambda_{SM})$,¹² we find the critical value for the top coupling $h_{c,0} = h_c(\Lambda_{SM})$. For example, for $\Lambda_{SM} = 10^{18}$ GeV, $h_{c,0} = 0.417$. RG scaling to the weak scale, we find a critical top quark mass

$$m_{t_c} = \left(174.7 \pm 3 + 2.2 \log_{10} \frac{\Lambda_{SM}}{10^{18} \text{GeV}} \right) \text{GeV}. \quad (28)$$

where the uncertainty ± 3 GeV comes from higher order contributions to RG scaling and to threshold corrections at the scale of the top quark mass. This critical point is denoted by an open circle in Figure 5. Contours of m_t and m_H are also shown in this figure by the near

full theory is likely to differ substantially from that of the SM, so that we expect the actual behavior to be more extreme than the two dashed curves of Figure 5.

¹²The choice of the Higgs boson mass as a boundary condition of the RG equation has negligible impact on $g_L(\Lambda_{SM})$ and $g_Y(\Lambda_{SM})$.

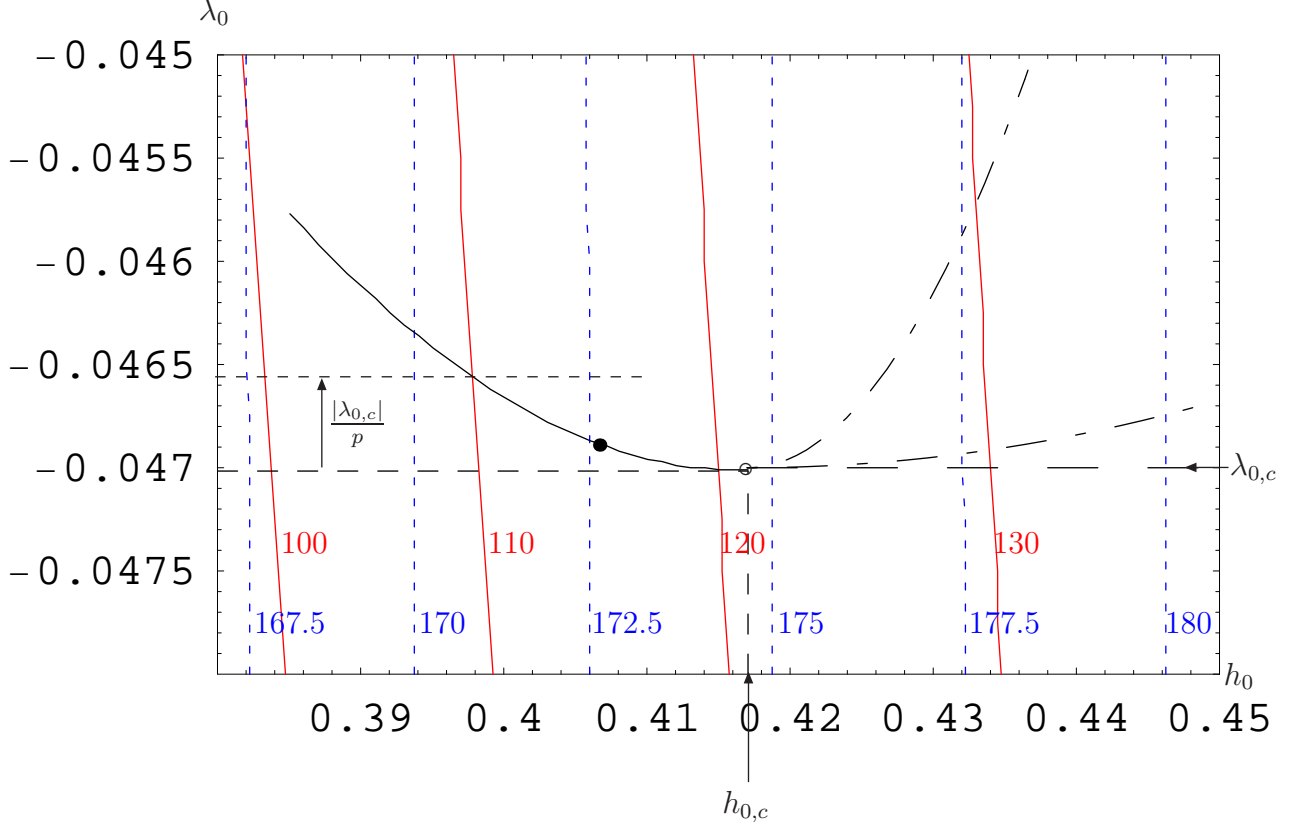


Figure 5: The metastability boundary in the λ_0 - h_0 plane for $\Lambda_{SM} = 10^{18}$ GeV. For $h_0 < h_{0,c}$ the solid curve is reliably computed in the SM. For $h_0 > h_{0,c}$, the metastability boundary must lie above the dashed horizontal line. Two possible boundaries are shown; the lower (upper) dot-dash curve results when tunneling in the full theory is suppressed (rapid). The nearly vertical blue dotted lines are contours of the top mass in 2.5 GeV intervals, while the red solid lines, also not far from vertical, are contours of the Higgs mass with 10 GeV intervals, shown for $\alpha_s = 0.1176$. The open circle is the critical point, giving the most probable observed values of m_t and m_H in the multiverse, corresponding to trajectory B of Figure 4b. The closed circle represents a patch of the multiverse on the metastability boundary where the top quark is measured to be 172.5 GeV. In our patch, the top mass is within a couple of GeV of this number, and hence lies somewhere between the m_t of 170 GeV and 175 GeV contours. The importance for the Higgs mass prediction of decreasing the experimental uncertainties on m_t is clear. An arrow denotes the magnitude of the expected upward fluctuations of the quartic coupling λ_0 above its critical value for peaking parameter $p = 100$. Such a fluctuation above $\lambda_{0,c}$ would lead to a point on the metastability boundary where the top mass is about 171 GeV and the Higgs mass about 110 GeV.

vertical blue dotted and red solid lines. Clearly a crucial question is how far from the critical point a typical patch in the false vacuum is likely to be.

3.3 The Width of the Top Mass Prediction

We would next like to determine how far from m_{t_c} the top mass could go, $\Delta m_{t\pm}$, before the probability would have fallen by a factor of e . In order to lower the top Yukawa h_0 below its critical value $h_{0,c}$, the Higgs quartic must be raised to prevent the RG flow of λ from heading into the forbidden region. This costs probability through the Higgs quartic probability distribution. As in section 2, we lose a factor of e in probability when the Higgs quartic is raised above the metastability boundary by an amount $|\lambda_c|/p$. The lower bound on the top mass prediction then corresponds to the smallest top Yukawa coupling compatible with this raised value of λ , and can be read off from the solid curve of Figure 5. For a small deviation from the critical point $(\lambda_{0,c}, h_{0,c}) = (-0.047, 0.417)$, the metastability boundary rises as $(\lambda_0 - \lambda_{0,c}) \simeq 1.24(h_0 - h_{0,c})^2$, and the downward shift $\Delta h_0 \sim \sqrt{|\lambda_{0,c}|/(1.24p)}$ or $\Delta h_{0,c}/h_{0,c} \sim 0.47/p$ gives the lower bound. Running down to the weak scale, $\Delta h/h$ shrinks by a factor of 0.4, and we find a corresponding downward shift in the top mass of

$$\Delta m_{t-} \approx \frac{35 \text{ GeV}}{\sqrt{p}}. \quad (29)$$

Such a shift is illustrated and discussed in Figure 5 for $p = 100$.

The upper bound on the top mass prediction is less certain; it depends on either the shape of the $\lambda - h$ metastability boundary to the right of the critical point, or on the strength, given by q , of the the fundamental probability distribution on h . In the former case, the upper bound depends on unknown physics beyond Λ_{SM} and we cannot make a quantitative statement. In the latter case the probability will have dropped by a factor of e for a top Yukawa that is above the critical value by an amount $\approx h_c/q$, corresponding to

$$\Delta m_{t+} \approx \frac{75 \text{ GeV}}{q}. \quad (30)$$

Putting everything together, our final result for the top mass prediction is

$$m_t = \left(174.7 \pm 3 + 2.2 \log_{10} \frac{\Lambda_{SM}}{10^{18} \text{ GeV}} - \frac{3}{\sqrt{p/135}} + \frac{3}{q/25} \right) \text{ GeV}. \quad (31)$$

We find this to be a striking success. Indeed, for the agreement with experiment not to be accidental, the a priori distribution for λ_0 must be highly peaked, certainly with $p \gtrsim 20$, so that the uncertainty in the Higgs mass prediction from the landscape, (18), is less than 1 GeV.

4 Higgs Mass Prediction from Thermal Fluctuations

All the analysis in the preceding sections assumed that the temperature of the thermal plasma remained sufficiently small after the last era of inflation. On the other hand, thermal fluctuations can themselves induce vacuum transitions from the false vacuum with $\langle H \rangle = v$ to the true vacuum with large $\langle H \rangle$. If the temperature was sufficiently high, then the vacuum transitions are dominated by these thermal processes, not by the quantum tunneling discussed so far [22, 23, 18, 24]. This section investigates how the results in the earlier sections should be modified in this case. We will continue to assume that the Standard Model is a good approximation up to a very high scale, and will return to the assumption that the top quark Yukawa coupling does not effectively scan in the landscape.

4.1 Vacuum Transitions at High Temperatures

As the inflaton decays, the inflation vacuum energy density V_I is converted into a thermal plasma. The maximum temperature of this plasma will be denoted by T_{\max} , which we will assume to be less than Λ_{SM} . The reheating temperature, at which the thermal plasma dominates the energy density of the universe, will be denoted by T_R . In the simplest scenarios for reheating, we have the relation $T_{\max}^4 \sim \sqrt{T_R^4 V_I}$. Note that since tensor perturbations have not yet been observed in the cosmic microwave background, an upper bound has been placed on V_I of about $(10^{16} \text{ GeV})^4$.

The vacuum decay rate induced by thermal fluctuations is again calculated by expanding around a bounce solution. The Higgs potential now involves a thermal contribution in addition to the one at $T = 0$:

$$V_{\text{tot}}(H) = \frac{\lambda(H)}{4} H^4 + V_{TH}(H; T). \quad (32)$$

The quartic potential with negative λ does not have an SO(3)-symmetric bounce solution. A bounce exists only for the total potential (32). The potential does not have a conformal symmetry at all, and as a result, bounces to field values of order T dominate in the decay rate, and the bounce action depends only on $\lambda(T)$. This is to be contrasted with the situation in section 2, in which tunneling to all scales had to be summed up, and the entire RG trajectory $\lambda(\mu)$ was important for tunneling at any given time. It should be noted, though, that since the temperature of the universe changes, the full RG behavior of $\lambda(\mu)$ up to $\mu = T_{\max}$ will still be important in this section, through the time dependence of the temperature.

We will now perform an analysis at a somewhat low level of approximation to get an overall qualitative picture of what is going on. For precise quantitative results, numerical calculations

will be used, as can be seen in what follows. We will employ the approximation adopted by [23]; for $g_{\text{eff}}H \ll T$, the high-temperature (H/T) expansion of the potential may be used. The leading term of the 1-loop thermal potential is then the thermal mass term

$$V_{\text{TH}}^{(2)} \simeq \frac{1}{2}g_{\text{eff}}^2 T^2 H^2, \quad (33)$$

where

$$g_{\text{eff}}^2 \equiv \frac{1}{12} \left(\frac{3}{4}g_Y^2 + \frac{9}{4}g_L^2 + 3h^2 \right). \quad (34)$$

For $\lambda(T)$ negative and $g_{\text{eff}}^4 \ll |\lambda(T)|$, the potential barrier for the transition occurs at around $H \sim g_{\text{eff}}T/\sqrt{|\lambda(T)|}$. Thus $g_{\text{eff}}H$ is in this case much less than T , so that the high-temperature expansion is a good approximation. Reference [23] then obtained

$$\frac{S_3}{T} \simeq \frac{6.015\pi g_{\text{eff}}(T)}{|\lambda(T)|}, \quad (35)$$

and a corresponding thermal decay rate per unit volume of

$$\Gamma[\lambda(T); T] \simeq T^4 \left(\frac{S_3}{2\pi T} \right)^{3/2} e^{-\frac{S_3}{T}}. \quad (36)$$

In order to determine the probability of a point remaining in the false vacuum at a time t , one must consider the possibility of bubble nucleations throughout the point's past light-cone. The result for the fraction of the universe in the false vacuum at time t is then [14]

$$f(\lambda_0; t) = \exp \left(- \int_{t_{\text{init}}}^t dt_1 \Gamma[\lambda(T(t_1)); T(t_1)] a(t_1)^3 \frac{4\pi}{3} \left\{ \int_{t_1}^t \frac{dt_2}{a(t_2)} \right\}^3 \right), \quad (37)$$

where t_{init} is the time right after the end of inflation, and $a(t)$ is the scale factor of the expansion of the universe. In fact, the same equation was used in section 2 as a precursor to (10). Here, however, Γ changes as the temperature of the universe changes, and so we must now use the more general expression. Assuming a standard thermal history after the end of inflation, namely, a matter-dominated era of inflaton coherent oscillations, followed by radiation domination and matter domination (and further dark-energy domination), we obtain

$$f(\lambda_0; t) \sim \exp \left(- \int_{T_R}^{T_{\text{max}}} \frac{dT}{T} \Gamma[\lambda(T); T] \frac{M_{\text{Pl}} T_R^2}{T^4} \left(\frac{T_R}{T} \right)^8 \left(\frac{T(t)}{T_R} \right)^3 t^3 - \int_{\lambda(T)<0}^{T_R} \frac{dT}{T} \Gamma[\lambda(T); T] \frac{M_{\text{Pl}}}{T^2} \left(\frac{T(t)}{T} \right)^3 t^3 \right), \quad (38)$$

assuming that t is in the recent matter-domination era.¹³ Here, T_{eq} is the temperature of matter-radiation equality, and $T(t)$ is the photon temperature at time t . We have used $T^4 \propto 1/a(t)^{3/2}$ and $dt \sim -(M_{Pl}T_R^2/T^4)(dT/T)$ during the inflaton dominated era [25]. Coefficients of order unity are ignored in the above expression for f , for the same reason as in section 2.

One can introduce a critical value of the Higgs quartic coupling $\lambda_c(T)$ by

$$\Gamma[\lambda_c(T); T] \tau^3 \frac{M_{Pl}}{T^2} \left(\frac{T_R}{T}\right)^{10} \left(\frac{T_0}{T_R}\right)^3 \simeq 1, \quad T_R < T, \quad (39)$$

$$\Gamma[\lambda_c(T); T] \tau^3 \frac{M_{Pl}}{T^2} \left(\frac{T_0}{T}\right)^3 \simeq 1, \quad T < T_R, \quad (40)$$

where¹⁴ $T_0 \simeq 2.73 \text{ }^\circ\text{K} \simeq 2.35 \times 10^{-4} \text{ eV}$ and $\tau = 10^{10}$ yrs. By taking a logarithm and using (36), we have¹⁵

$$\frac{6.0\pi g_{\text{eff}}(T)}{|\lambda_c(T)|} \simeq \ln\left(\frac{M_{Pl}}{T}(\tau T_0)^3\right) + \frac{3}{2} \ln\left(\frac{S_3}{2\pi T}\right) + \left[7 \ln\left(\frac{T_R}{T}\right)\right], \quad (41)$$

$$\text{or equivalently} \quad \lambda_c(T) \simeq -\frac{6.0\pi g_{\text{eff}}(T)}{243 - \ln\frac{T}{v} - \left[7 \ln\frac{T}{T_R}\right]}. \quad (42)$$

The term $[7 \ln(T/T_R)]$ is in square brackets because it should be included only when $T > T_R$. The critical line of stability $\lambda_c(T)$ is shown in Figure 6, along with some RG trajectories of the Higgs quartic coupling for $m_t = 172.5 \text{ GeV}$. If an RG trajectory passes below the critical line at an energy scale $\mu < T_{\text{max}}$, we will have $f(\lambda_0; t) \ll 1$, so that most patches of the universe with the corresponding Higgs boson mass would have decayed to the true vacuum by now.

In Eq. (42), $g_{\text{eff}}(T)$, as calculated from (34), lies in the range 0.3–0.4 for a wide range of T . At the same time, $|\lambda_c(T)|$ ranges from 0.03–0.04, so that $|\lambda_c(T)|$ is not much bigger than g_{eff}^4 . For this reason, the high-temperature expansion of the thermal potential is not particularly good, and consequently, $6.0\pi g_{\text{eff}}/|\lambda|$ is not actually a very good estimate for the bounce action

¹³If t is in the era of cosmological constant dominance that follows after the recent matter-dominance era, then $T(t)^3 t^3$ is replaced by $T_{eq}'^3 H_0^{-3}$ for $t \gg t'_{eq}$, where T_{eq}' and t'_{eq} are the temperature and epoch of matter-cosmological constant equality, and H_0 is the Hubble constant of the cosmological constant. Note that the t -dependence completely disappears from $f(\lambda_0; t)$.

¹⁴Factors of order unity are not important here, since these equations balance a very small Γ against a very large $\tau^3 M_{Pl}/T^2$. In particular, it is not important whether we are in the dark-energy dominated era or not, or which values to use for τ and T_0 . A factor of 2–3 changes $\lambda_c(T)$ by half percent, which corresponds to less than 0.1 GeV change in the Higgs boson mass.

¹⁵The number “243” contains $(3/2) \ln(243/2\pi) \simeq 5.5$ that comes from the 1-loop functional determinant. Note that ΔS of section 2, also calculated from a 1-loop functional determinant, contributed a similar order of magnitude, ~ -10 [4].

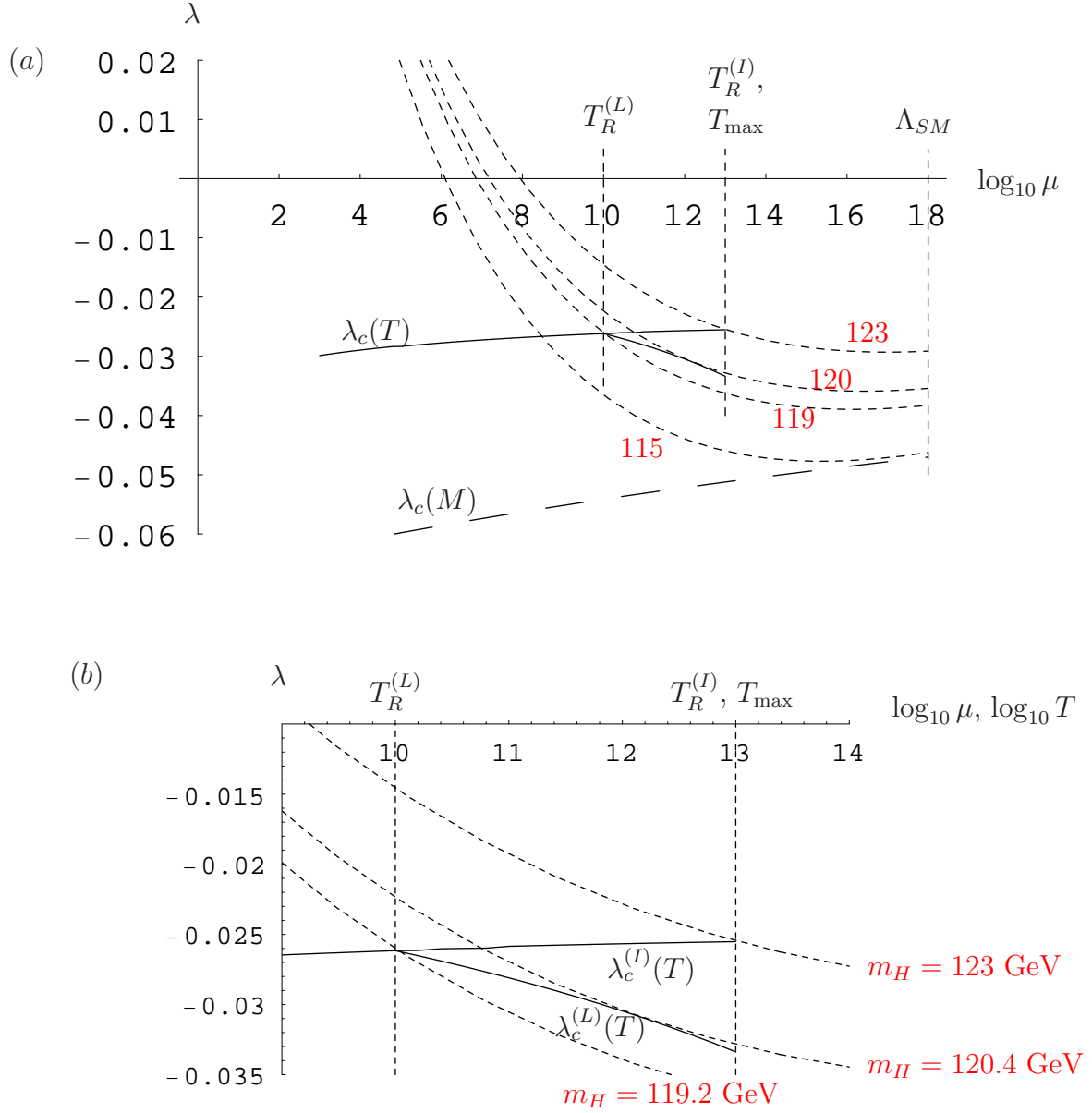


Figure 6: The critical line of stability due to vacuum decay by thermal fluctuations, shown as solid lines terminating at T_{\max} . Two cases are shown, both with $T_{\max} = 10^{13}$ GeV. The upper solid line, case (I), corresponds to instantaneous reheating with $T_R = T_{\max}$. Varying $T_R = T_{\max}$ away from 10^{13} GeV will simply change the termination point of the line. The lower solid line, case (L), corresponds to late reheating with $T_R = 10^{10}$ GeV. Varying T_R will alter the position of the bend in the line, while altering T_{\max} will alter the termination point. The two lines coincide for $T < 10^{10}$ GeV. The long dashed line near the bottom is $\lambda_c(M)$ discussed in section 2. Four RG trajectories of $\lambda(\mu)$ are also shown, as dotted lines, with Higgs masses of (115, 119, 120, 123) GeV. The lower panel is a blow-up of the upper panel. The low temperature value of the critical Higgs mass, 115 GeV, is raised to 120 GeV in case (L) and 123 GeV in case (I).

S_3/T [24]. The critical line of stability in Figure 6 was therefore obtained from a numerical calculation, the details of which are explained in the appendix. On the other hand, expression (42) does capture the qualitative behavior of $\lambda_c(T)$ shown in the figure. For $T < T_R$, the asymptotically free behavior of the $SU(2)_L$ and top Yukawa couplings are more important than the $-(1/243)\ln(T/v)$ term in the denominator, and $|\lambda_c(T)|$ slowly decreases as T increases. For $T > T_R$, however, the extra $-(7/243)\ln(T/T_R)$ term in the denominator is more important, and $|\lambda_c(T)|$ increases.

Figure 6 shows $\lambda_c(T)$ for two scenarios: one for $T_{\max} = T_R = 10^{13}$ GeV, and the other for $T_R = 10^{10}$ GeV and $T_{\max} = 10^{13}$ GeV. In the instantaneous reheating scenario at $T = 10^{13}$ GeV (I), an RG trajectory of $\lambda(\mu)$ with $m_H = 123$ GeV (upper dotted curve in Figure 6b) touches the line of $\lambda_c^{(I)}(T)$ at $T \simeq 10^{13}$ GeV. Patches of the universe with Higgs boson masses smaller than 123 GeV would have mostly decayed because their RG trajectories pass below the $\lambda_c^{(I)}(T)$ line at some temperature less than T_{\max} . In the late reheating scenario with $T_R = 10^{10}$ GeV (L), the RG trajectory for $m_H = 120.4$ GeV (middle dotted curve in Figure 6b) touches $\lambda_c^{(L)}(T)$ at a temperature in between T_R and T_{\max} . Thus, in this case patches of the universe with $m_H < 120.4$ GeV typically decayed to the true vacuum within the inflaton dominated era. It is clear from Figure 6a that the constraint from vacuum decay due to quantum fluctuations, shown as a long dashed line, is of negligible importance for both (I) and (L) scenarios discussed above, as well as many other cases with high T_R .

4.2 The High Temperature Prediction for the Higgs Boson Mass

When the a priori distribution $P(\lambda_0)$ of the Higgs quartic coupling is highly peaked toward negative values, a balance between $f(\lambda_0; t)$ and $P(\lambda_0)$ determines the most likely value of the Higgs boson mass. Since the double-exponential cut-off in f is so sharp, again the point of maximum probability occurs essentially at the cut-off, as in section 2. Thus, the phenomenological lower bound on the Higgs boson mass may again become the prediction of a landscape scenario.

Let us now consider a case with $T_R = 10^{10}$ GeV as an example. If T_{\max} is also 10^{10} GeV, then f sets a cut-off $\lambda(10^{10} \text{ GeV}) > \lambda_c(10^{10} \text{ GeV}) \simeq -0.026$, as we see from Figure 6b. The RG trajectory with $\lambda(\mu = 10^{10} \text{ GeV}) = -0.026$ becomes the landscape prediction, which corresponds to $\bar{m}_H = 119$ GeV. If T_{\max} is a little higher than 10^{10} GeV, patches with $m_H = 119$ GeV have mostly decayed during the inflaton-oscillation dominated era, because the RG trajectory lies below the critical line of stability $\lambda_c^{(L)}(T)$. Thus the prediction for m_H goes up as T_{\max} increases. For sufficiently high T_{\max} , however, this sensitivity to T_{\max} disappears; the

RG trajectory with $m_H = 120.4$ GeV touches $\lambda_c^{(L)}(T)$ at around 10^{12} GeV. As long as T_{\max} is higher than this temperature, the landscape prediction will remain at $\overline{m}_H = 120.4$ GeV. Figure 7 shows the prediction for the most probable Higgs mass \overline{m}_H in these two limits, the instantaneous reheating scenario, with $T_{\max} = T_R$, and the high $T_{\max} \gg T_R$ scenario. The prediction will always lie in between these two lines for any T_{\max} .

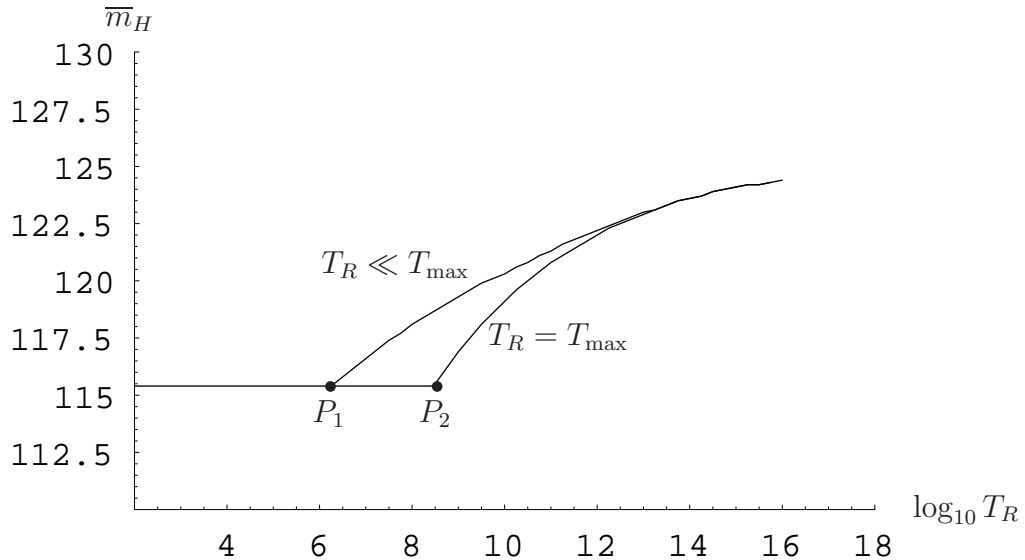


Figure 7: The prediction for the central value of the Higgs boson mass as a function of the reheating temperature T_R . The upper line is for the $T_{\max} \gg T_R$ scenario, and the lower line for the instantaneous reheating scenario, $T_{\max} = T_R$. We assume that the top Yukawa coupling is fixed in the landscape, so that $m_t = 172.5$ GeV. Note that the ± 6 GeV error bar in (15), coming from threshold corrections at the weak scale etc., is not shown.

Now, for sufficiently high reheating temperature, $T_R \gtrsim 10^{13}$ GeV, the prediction does not depend on T_{\max} at all. This is because the RG trajectories for $\lambda(\mu)$ run almost horizontally at high energies, and touch the critical line of stability $\lambda_c(T)$ at the bend at $T = T_R$ (see Figure 6). Vacuum decay becomes most effective at the epoch of reheating in this case, and it does not matter how high T_{\max} is. The fact that the RG trajectories for λ run almost horizontally at high energies also explains why the prediction for m_H levels off and depends only weakly even on T_R at high reheating temperatures. The Higgs quartic coupling does not run much at high energies because of the smaller top Yukawa coupling.

Figure 6a shows that the RG trajectory corresponding to the prediction of section 2 (the lowest trajectory) crosses $\lambda_c(T)$ at around $\mu = 10^8$ – 10^9 GeV. Thus, the prediction of section 2

is unaffected if $T_R = T_{\max} \lesssim 10^8\text{--}10^9$ GeV in the instantaneous reheating scenario, as shown by point P_2 in Figure 7. The highest reheating temperature for which the prediction of section 2 persists actually depends on the relation between T_R and T_{\max} . The higher T_{\max} is, the lower the maximum value of T_R for which the vacuum prediction applies. In the limit $T_{\max} \gg T_R$, this value of T_R drops to around 10^6 GeV, as shown by point P_1 in Figure 7.

Finally, we have a few remarks about the uncertainties associated with the calculations of this section. The landscape prediction (15) in section 2, was derived from a value of the Higgs quartic coupling at a very high energy scale, M_{dom} . The three sources of uncertainties quoted in (15), namely, the measured top quark mass, QCD coupling and calculation of electroweak threshold corrections, potentially changed the relation between $\lambda(M_{dom})$ and m_H . The prediction in Figure 7 from the thermal scenario came from couplings renormalized at a lower energy scale $\sim T \ll M_{dom}$. However, the running of $\lambda(\mu)$ takes place mainly at low energy, where the top Yukawa coupling is large. Thus, the prediction for the Higgs mass at high reheating temperature is also subject to the same three uncertainties quoted in (15) with almost equal sizes. The influence of the details of the 1-loop functional determinant was at most 1 GeV [4] for the prediction in (15), and it will remain at that order of magnitude in Figure 7 as well, because the estimates of the 1-loop functional determinant are much the same; see footnote 15.

It should be noted that the prediction in the case of high reheating temperature is associated with an additional uncertainty: the precision of the calculation of the thermal effective potential. This issue is briefly discussed in the appendix.

4.3 The Width of the High Temperature Prediction

The width of the Higgs mass prediction for this section may be obtained similarly to that of section 2. We consider the total probability $\mathcal{P} = Pf$, and again we may define λ_- and λ_+ to be the values of the quartic coupling at Λ_{SM} for which \mathcal{P} has fallen from its peak value by a factor of $1/e$. Since the cut-off from f is so sharp, λ_- is again a negligible distance from the peak. As in section 2, λ_+ is shifted above the critical value λ_c by an amount $|\lambda_c|/p$, where here we are using the value of the critical quartic coupling run up to the scale Λ_{SM} . p is defined as in section 2 by $p = \left. \frac{\partial \ln P(\lambda_0)}{\partial \ln \lambda_0} \right|_{\lambda_0=\lambda_c}$. This yields a possible upwards shift in the Higgs mass of

$$\Delta m_H \approx \frac{500|\lambda_c|\text{GeV}}{p}. \quad (43)$$

Here, $|\lambda_c|$ ranges from about .02 to .05 depending on the particular thermal history after inflation. This gives an upwards shift between $(\sim 10 \text{ GeV})/p$ and $(\sim 25 \text{ GeV})/p$.

4.4 Discussion

In the case that SM patches of the universe were reheated to very high temperatures after inflation, our prediction for the central value of the Higgs boson mass is shown in Figure 7. Despite a very wide range in the cosmologies considered, the central value remains in the region (115–125) GeV. Furthermore, for $T_R < 10^6$ GeV thermal fluctuations are irrelevant and the 115 GeV result from quantum tunneling applies, while for $T_R > 10^{12}$ GeV, the prediction is in the narrow range (123 ± 1) GeV. The uncertainties from the experimental values of m_t and α_s and from higher loop orders are closely similar to those in the non-thermal case. The peaking of the a priori distribution for λ_0 yields an upper width on the prediction that is higher than the central value by an amount between ~ 10 GeV/ p and ~ 25 GeV/ p , depending on the reheat temperature.

The top mass prediction of section 3 is very significant. If the top Yukawa coupling h_0 is allowed to scan, does this prediction survive thermal fluctuations at high temperatures? If $T_R > 10^9$ GeV, then a large p will cause h_0 to rise significantly above the observed value, since a larger h_0 gives both a steeper quartic trajectory and a lower $\lambda_c(T)$ curve. Thus, to maintain the highly significant m_t prediction from section 3, we are led to a preference for low T_R and a central Higgs mass of 115 GeV.

5 The Scanning Standard Model

Consider the SM, minimally augmented with right-handed neutrinos to allow for both neutrino masses and leptogenesis, with all parameters scanning—the scanning SM. It is possible that hospitable parts of the landscape exist where parameters take on values that are very different from the ones we observe. This is well-illustrated by the weakless universe [26], where $\langle H \rangle / M_{Pl} \approx 1$ while the Yukawa couplings for the light quarks and the electron, $h_{u,d,s,e}$, are all less than 10^{-20} . We assume that, if such regions exist, they are less probable than our own universe. For example, the weakless universe may be disfavored because of a very small probability to have four Yukawa couplings that are so small. In the landscape, the origin for $v \ll M_{Pl}$ may be that a small value for v is the most cost effective way of keeping u, d, s and e light. Hence the question becomes: in our neighborhood of the landscape, how much of the parameter space of the scanning SM can be understood from environmental selection? We have argued that the entire Higgs potential is strongly selected, and now we turn to the Yukawa coupling matrices, where most of the parameters lie. In sections 2, 3, and 4 we have been exclusively focused on precise predictions for the Higgs and top masses. In this section we explore possible

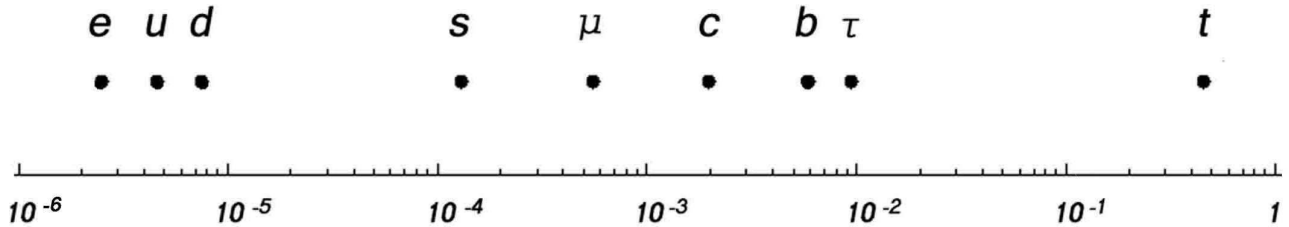


Figure 8: The Yukawa couplings for the quarks and charged leptons scaled up to 10^{18} GeV, and plotted logarithmically. The environmentally important e, u, d and t couplings seem to be outliers, while the remaining five couplings are all clustered in a two order of magnitude range.

consequences of embedding our previous results into the scanning SM. Further assumptions are found to lead to intriguing order of magnitude estimates for a variety of quantities.

5.1 Quark and Charged Lepton Masses

Let us first ignore flavor violation and consider scanning of the nine charged fermion eigenvalues. In Figure 8 we plot the nine Yukawa couplings of the SM at the renormalization scale $\Lambda_{SM} = 10^{18}$ GeV. They fall into three well separated groups: the e, u and d Yukawas, selected to be small by the requirement that atoms exist [31], the t coupling, selected to be large to avoid vacuum instability, and the remaining five Yukawa couplings that are environmentally irrelevant, and therefore reflect the underlying probability distribution on the landscape. It is striking that while the nine couplings span 5 orders of magnitude, the five irrelevant couplings span only 2 orders of magnitude. It therefore seems possible to make progress on the fermion mass hierarchy problem by assuming a universal fermion Yukawa eigenvalue probability distribution that is peaked around 10^{-3} , with a width of one to two orders of magnitude. Possible simple analytic forms for the distribution include

$$P(\tilde{h}) = A e^{-\left(\frac{\log_{10} \tilde{h}}{\sqrt{2}\sigma}\right)^2} \quad (44)$$

with $\tilde{h} = h_0/10^{-3}$ and $\sigma \simeq 0.75$, and

$$P(\tilde{h}) = A \tilde{h} e^{-\tilde{h}}. \quad (45)$$

Thus the five irrelevant Yukawa couplings are scattered logarithmically about 10^{-3} , while the four outliers are environmentally selected to be far from the peak of the distribution.¹⁶ This

¹⁶With these distributions, the weakless universe is indeed much less probable than the observed SM.

interpretation of the data of Figure 8 seems so plausible, that we investigate further the role of electroweak phase stability in forcing the top coupling to large values.

From Figure 2 it is clear that if a strongly peaked distribution $P(\lambda_0)$ pushes λ_0 towards its critical value $\lambda_{0,c}$, then vacuum instability is only avoided if there is a Yukawa coupling that is sufficiently large to RG scale λ to positive values by the weak scale. This can be accomplished by a large top coupling via the term $-6h_t^4$ of (7). However, with all Yukawa couplings scanning, the $-6h_t^4$ term could be replaced by other large Yukawa contributions. One easily sees that it is more probable to have a single large Yukawa rather than two or more large Yukawas making significant contributions to the quartic RG equations. Furthermore, it is not sufficient for the single large Yukawa to be that of a lepton: it is only for a quark that QCD increases the Yukawa in the infrared, thus magnifying the effect on the scalar quartic coupling. The critical value for a lepton Yukawa coupling is slightly larger than for a quark, but this is insufficient to allow a critical quartic coupling at Λ_{SM} to become positive by the weak scale. Hence, our simple interpretation of Figure 8, in terms of a universal $P(h_0)$ and environmental selection of outliers, predicts not only that there will be a single heavy fermion, but that it must be a quark. However, the choice of up-like versus down-like is random. Crucially, as we have shown in section 3, a precise and successful prediction for the top quark results.¹⁷

If this picture of fermion masses is correct, then there is a further consequence for the u, d and e masses. Since they are selected to be quite far from their most probable values in the landscape, our patch of the universe is quite rare. This means that they are expected to be quite close to the maximum values consistent with environmental selection for the existence of complex atoms. Of course, this is sensitive to the actual probability distribution for the Yukawa couplings. For example, using the distribution (44) patches in the multiverse with the electron Yukawa double its observed value are more than an order of magnitude more probable than in our patch. On the other hand, for the distribution (45) they are only twice as probable.

It is not clear how the small CKM mixing angles could arise from environmental selection. Vacuum stability has selected an up-type quark to be heavy, and nuclear physics has selected a down-type quark to be light. In nature these two quarks are almost precisely in different weak doublets, so that $V_{td} \simeq 10^{-3}$, but there does not appear to be a selection effect to explain this. This is similar, but numerically more severe, to the puzzle of why environmental selection would make V_{ud} close to unity. Quark flavor violation appears to be governed, at least to

¹⁷Note that the distribution (44) gives a peaking parameter $q \simeq 2$. While this has the right sign to limit Δm_{t+} , the size of Δm_{t+} from (30) seems too large. Hence, either $P(h)$ drops more rapidly at large h compared to (44), or Δm_{t+} is made small by a large tunneling rate in the full theory above Λ_{SM} .

some degree, by symmetries. Numerical simulations of Yukawa matrices have been made for very flat landscape probability distributions [27]. It would be interesting to perform numerical simulations using more peaked distributions, such as (44) or (45), and incorporating elements of approximate flavor symmetries.

5.2 Neutrino Masses, Leptogenesis and Inflation

Since no large neutrino mass ratios or very small neutrino mixing angles have been measured, it is very plausible that the entries of the neutrino mass matrices, both Dirac and Majorana, are distributed according to some universal probability distribution of the landscape. Indeed, Neutrino Anarchy demonstrated in some detail how randomly generated neutrino mass matrices could account well for the observed masses and mixings [28]. The view of the charged fermion masses presented above has an important consequence for neutrino physics. We assume that the Dirac neutrino Yukawa couplings are governed by the same landscape probability distribution as the quarks and charged leptons. If there is little environmental selection acting on the neutrinos, then the typical Dirac Yukawa eigenvalue \bar{h}_ν is expected to be of order 10^{-3} in magnitude.¹⁸ Since no large hierarchy of neutrino masses is observed, it is reasonable to also assume that the three Majorana masses of the right-handed neutrinos are governed by a universal probability distribution, so that they are all expected to have a common order of magnitude, \bar{M}_R . With $\bar{h}_\nu \approx 10^{-3}$, there is a relation between \bar{M}_R and the order of magnitude of the light neutrinos, \bar{m}_ν :

$$\frac{\bar{m}_\nu}{\text{eV}} \approx \frac{3 \times 10^7 \text{ GeV}}{\bar{M}_R} \left(\frac{\bar{h}_\nu}{10^{-3}} \right)^2 \quad (46)$$

In our patch of the multiverse, \bar{m}_ν has been observed to be of order 10^{-2} eV, so that we predict

$$\bar{M}_R \approx 3 \times 10^9 \text{ GeV} \quad (47)$$

in our patch.

Leptogenesis is the only possible source of a baryon asymmetry in the scanning SM. Is it consistent with our framework for fermion masses? The lepton asymmetry is given by [29]

$$Y_L \approx \kappa \frac{\epsilon_1}{g_*}, \quad (48)$$

where $g_* \simeq 100$ counts the number of states in the thermal bath. The CP asymmetry ϵ_1 and

¹⁸Sufficiently small that these couplings do not upset the prediction for the Higgs boson and top quark masses.

the washout factor κ are roughly of order

$$\epsilon_1 \sim \frac{3}{16\pi} \bar{h}_\nu^2 \sim 10^{-1} \bar{h}_\nu^2, \quad \kappa \sim 10 \frac{1}{\bar{h}_\nu^2} \frac{\bar{M}_R}{M_{Pl}}, \quad (49)$$

respectively, where we have assumed comparable masses for the right-handed neutrinos. We are now assuming that all relevant entries of the neutrino Yukawa coupling matrix are of order \bar{h}_ν . We see that the observed baryon asymmetry is roughly reproduced after using (47):

$$Y_L \approx 10^{-11} \left(\frac{\bar{M}_R}{3 \times 10^9 \text{ GeV}} \right) \approx 10^{-11} \left(\frac{\bar{h}_\nu}{10^{-3}} \right)^2 \left(\frac{10^{-2} \text{ eV}}{m_\nu} \right). \quad (50)$$

This can be regarded as an indication that the Dirac Yukawa couplings of neutrinos are also subject to the universal distribution $P(h_0)$ of Yukawa couplings.

The baryon asymmetry is roughly derived from the observed low-energy neutrino masses, or vice versa; either one of them can be used as an input so that the other is determined. Now the next question is whether we can understand them all together environmentally. Suppose that the Majorana masses of the right-handed neutrinos are scanned. The distribution of M_R may be a featureless flat distribution, like that of the cosmological constant; or, the baryon asymmetry, being proportional to M_R (as in (50)), may put more weight on larger values of M_R . We assume that the distribution of M_R is mildly peaked toward larger values. If the reheating temperature T_R is also scanned mildly, but with an a priori distribution peaking weaker than that of M_R , then both M_R and T_R would go hand in hand, pushed upward, because the baryon asymmetry is at least power-suppressed when T_R is much lower than M_R . Both M_R and T_R go up until T_R and T_{max} are so high that the Higgs vacuum becomes unstable. If T_{max} is also scanned, with an even milder a priori distribution, T_R will be pushed upward along the line from P_1 to P_2 in Figure 7 until it reaches the special point P_2 . For a large p , on the other hand, a reheating temperature higher than that is less probable, because a large p strongly favors a smaller λ_0 , which is environmentally allowed only in patches with lower T_R . Thus environmental selection for the desired electroweak vacuum, on the combined a priori probability distribution, leads to the special point P_2 as the most likely one to be observed, and hence to the predictions

$$T_R \approx T_{\text{max}} \approx 10^8\text{--}10^9 \text{ GeV}. \quad (51)$$

Since $T_{\text{max}}^4 \approx \sqrt{T_R^4 V_I}$, we predict the vacuum energy during inflation

$$V_I \approx (3 \times 10^8 \text{ GeV})^4 \quad (52)$$

corresponding to a Hubble parameter during inflation of order 10^{-2} GeV. These speculations will clearly be disproved if a tensor perturbation is seen in the cosmic microwave radiation. From the reheat temperature we predict the decay rate of the inflaton

$$\Gamma_I \approx 10^{-2} \text{ GeV}. \quad (53)$$

Now that the rough scale of M_R is obtained without an observational input, low-energy neutrino masses of order 10^{-2} eV and the baryon asymmetry are also purely predictions of environmental selection. The Higgs boson mass prediction still remains at 115 GeV, and the top mass prediction in section 3 is also maintained along the horizontal line of $m_H = 115$ GeV, where thermal transitions are not important.

Since in thermal leptogenesis the lightest right-handed neutrino mass can be slightly higher than the reheating temperature T_R , there is no conflict between T_R in (51) and \overline{M}_R in (47). Also, the neutrino Yukawa couplings contributing to the CP asymmetry ϵ_1 may fluctuate bigger, and those appearing in the denominator of the washout factor κ smaller, making the entire baryon asymmetry bigger. Thus an apparent discrepancy of one order of magnitude is nothing to worry about. Although the reheat temperature (51) does not satisfy the phenomenological limit $2 \times 10^9 \text{ GeV} < T_R$ derived from the observed baryon asymmetry [29], our estimates are only order of magnitude ones. Furthermore, this limit does not apply when the right-handed neutrinos have highly degenerate Majorana masses. An environmental factor $\propto Y_B$ may motivate such highly degenerate right-handed neutrinos.

5.3 Gauge Couplings

If all three SM gauge couplings scan, then α and α_s are selected, while the weak mixing angle $\sin^2 \theta$ is apparently environmentally irrelevant. However, the condition for the critical value for the top quark coupling, equation (27), depends on the weak mixing angle. Hence it is possible that avoiding vacuum instability could select for the weak mixing angle in addition to the top quark and Higgs masses! If the a priori probability distribution has a stronger dependence on h_t than $\sin^2 \theta$ then we find the incorrect prediction of $\sin^2 \theta \simeq 0.38$ at the weak scale. Hence it must be that the weak mixing angle is essentially determined by the landscape distribution.

Gauge coupling unification is possible in the scanning SM, with Λ_{SM} near M_{Pl} , if threshold corrections are of order 10–20%. Since the threshold corrections to the gauge coupling constants arise from dimension-5 operators, while the leading order correction to the Higgs potential (6) is a dimension-6 operator, corrections to gauge coupling unification can be as large as 10–20% without losing the 1%-level precision of the predictions in earlier sections.

5.4 Dark Matter

The final parameter of the SM that could scan is the strong CP parameter of QCD. It is attractive to promote this to the axion field, with an associated symmetry breaking scale above Λ_{SM} . It has been argued that scanning the primordial value of this axion field not only allows axionic dark matter, but could explain the approximate equality of dark matter and baryon energy densities [33].

The scanning SM is frustrating in the sense that there appears little that is amenable to experimentation beyond the Higgs mass prediction. However, the question of flavor in both quark and neutrino sectors is left unresolved, and in the neutrino sector more thought needs to be given to the environmental selection effects arising from leptogenesis.

We caution the reader that there are potential difficulties with the scanning SM that we do not address in this paper. For example, particle physics of the SM is completely unchanged if m^2 and the QCD scale Λ_{QCD}^2 are increased by the same factor, and corresponding changes are made to the dimensionless couplings so that their values at the scale m^2 are kept fixed. The environmental selection of the weak scale to be as small as 100 GeV would then be undermined, unless some probability distribution can be found to counteract the one favoring large m^2 , or some other environmental selection involving the Planck scale, such as big bang nucleosynthesis, limits such a scanning direction. Similar questions arise for the environmental selection of the cosmological constant when there is simultaneous scanning of other cosmological quantities, such as the density perturbations. This has been addressed by a consideration of other selection effects [30].

6 Conclusions and Discussion

There are many mass scales that play an important role in physics, for example the electron and proton masses, but from a fundamental viewpoint two are key: the scale of electroweak symmetry breaking, $\langle H \rangle = v$, that sets the mass scale of the quarks and leptons as well as the W and Z bosons, and the Planck mass, M_{Pl} , that describes the gravitational coupling and is the largest scale that enters physics. We take the viewpoint that the Planck scale is fundamental and the weak scale is somehow to be derived, although the alternative is also possible, so that the key question becomes the origin of the small dimensionless parameter v/M_{Pl} .

Over the last 30 years, many frameworks have been developed that can explain this small ratio by introducing various symmetries. The LHC is expected to play a crucial role in dis-

tinguishing between these frameworks, for example between supersymmetry and new strong forces at the TeV scale. The alternative viewpoint, that v/M_{Pl} is environmentally selected [8] and has nothing to do with extended symmetries, has received relatively little attention, perhaps because it leads to no new physics, beyond a light Higgs boson, to be discovered at LHC. Of course it is possible that in this case the LHC might discover physics unrelated to electroweak symmetry breaking, perhaps associated with either dark matter or coupling constant unification, but it is hardly to be expected. Dark matter is not necessarily related to the electroweak scale; axion dark matter with an environmentally chosen relic density is an example. Gauge coupling unification requires new particles other than a Higgs doublet, but those particles may be around the Planck scale, for instance. If the origin of v/M_{Pl} is environmental, then arguments for physics discoveries beyond the SM at LHC become tenuous.

Another fundamental mass scale of nature is the cosmological constant, Λ^4 . To date, theories beyond the SM have failed to provide a symmetry understanding for why Λ/M_{Pl} is so small: why it is so close to zero, and what determines the order of magnitude of the deviation from zero. A symmetry might assign a special meaning to a vanishing cosmological constant, and it might be possible to understand the observed size of the dark energy by constructing theories that implement a seesaw relation $\Lambda \approx v^2/M_{Pl}$. On the other hand, environmental selection explains *both* the extreme smallness of Λ *and* its order of magnitude, as measured by the dark energy density. The dark energy and the ratio v/M_{Pl} are environmentally selected if two parameters of the renormalizable Higgs quartic potential are scanned. These successes motivate us to think of scanning the entire Higgs potential. In this case, the Higgs quartic coupling, λ , and therefore the physical Higgs mass, scans. By deriving a prediction for the Higgs boson mass, the idea of the scanning Higgs potential can be tested.

Environmental selection requires an “edge” [21, 32]— a surface in the space of scanning parameters, such that on one side of the surface the formation of desired complex structures is greatly suppressed. We do not know enough about conceivable life forms to derive the precise types of complexity to be selected. However, the more general the requirement, the more plausible selection becomes. The selection of small values for Λ/M_{Pl} results from an edge that corresponds to formation of non-linear structures late in the universe. As Λ/M_{Pl} is increased beyond this edge, the probability of such structures forming is suppressed because they are subjected to inflation before they go non-linear. On the other hand, a small value for v/M_{Pl} is selected by the requirement that atoms exist. The requirement that atoms exist is much more specific than the requirement that large non-linear structures form, but it is not unreasonable. For our prediction of the Higgs boson mass, the relevant edge is the phase boundary that

separates a metastable phase with small $\langle H \rangle / M_{Pl} = v / M_{Pl}$ from a phase with $\langle H \rangle / M_{Pl} \approx 1$. This is less specific than requiring the existence of atoms: life probably requires objects that contain a large amount of information, and this may be accomplished best in a phase with a large M_{Pl}/v ratio.

An edge that allows environmental selection is not sufficient to make predictions; some knowledge of the a priori probability distribution for the scanning parameters is needed. In the absence of a calculation from a fundamental theory of the landscape, this requires an assumption. For the cosmological constant and weak scales, this assumption is extremely mild; it is sufficient to assume that the distributions are roughly flat and featureless, so that small values of these scales are exceedingly rare. For our Higgs mass prediction a non-trivial assumption is necessary: the probability distribution $P(\lambda)$ must be sufficiently peaked at low coupling that λ is expected to be near the metastability boundary.

Since our edge is a phase boundary, the position of the boundary, and therefore the Higgs mass prediction, depends on the thermal history of the universe, in particular on the reheat and maximum temperatures after inflation, T_R and T_{\max} , two of the most important parameters of post inflationary cosmology that are still largely unconstrained, and consequently one might expect that little can be said about the Higgs mass. In fact, no matter what the values of these two temperatures the most probable value of the Higgs mass is raised from 115 GeV to at most 124 GeV. Furthermore, if $T_{\max} = T_R \lesssim 10^8 - 10^9$ GeV the prediction is very insensitive to cosmology, as the danger of a phase transition is highest today and was negligible in the early universe, giving

$$m_H = 115 \text{ GeV} - (115 + 25/p) \text{ GeV}, \quad (54)$$

while for $T_R > 10^{12}$ GeV, nucleation at high temperature dominates, giving $m_H = 123 \pm 1$ GeV for any value of T_{\max} , with an upper fluctuation between $\sim (10/p)$ GeV and $\sim (25/p)$ GeV from the a priori distribution, depending on the reheat temperature. The full dependence of the prediction on T_R and T_{\max} is shown in Figure 7. The parameter p is the logarithmic derivative of $P(\lambda)$ evaluated at the phase boundary. Further uncertainties, displayed in equations (15) and (18), arise from the experimental uncertainty in the QCD coupling and the top quark mass, and also from use of perturbation theory in RG scaling of couplings and in relating couplings to physical masses. Ultimately, these uncertainties can be reduced; but the width of the Higgs boson mass distribution from the multiverse, parameterized by p , cannot be reduced. This width is comparable to the present uncertainties if $p \approx 3$, while if $p > 10$ it is practically negligible compared with other uncertainties.

The top quark plays a crucial role in electroweak symmetry breaking via the RG evolution

of the quartic coupling λ . If the top Yukawa coupling also scans, a further mild assumption also allows a prediction for the top quark mass. For $T_R < 10^8\text{--}10^9$ GeV, the most probable top quark mass is

$$m_t = [174.7 \pm 3 + 2.2 \log_{10}(\Lambda_{SM}/10^{18} \text{ GeV})] \text{ GeV}. \quad (55)$$

To limit fluctuations above this requires a further assumption, while downward fluctuations are $35 \text{ GeV}/\sqrt{p}$. The striking success of this result suggests that environmental selection may be at work in the Higgs potential, and that we may be lucky enough for p to be sufficiently large to give a precise Higgs mass prediction. Maintaining this prediction in the presence of thermal fluctuations also implies that $T_R \lesssim 10^8\text{--}10^9$ GeV, so that the preferred central value of the Higgs mass prediction is 115 GeV, as shown in (54).

We have argued that these Higgs and top mass predictions could occur in the scanning SM, where all SM parameters scan. Indeed a zeroth-order understanding of the charged fermion masses follows if all Yukawa couplings have a universal probability distribution centered on about 10^{-3} . An interesting extension to neutrino masses and leptogenesis follows if right-handed neutrino masses scan, with a preference for larger values, and if T_R and T_{max} scan with mild distributions. The broad order of magnitude of the light neutrino masses and the baryon asymmetry are correctly predicted, while the right-handed neutrino masses, the reheat temperature and the maximum temperature are all predicted to be of order 10^9 GeV.

The possibility of precise predictions for the Higgs and top masses by environmental selection from a landscape illustrates that it may be possible to do physics without symmetries. Theories based on symmetries yield predictions because the symmetries limit the number of free parameters. One chooses a highly symmetric model and studies the resulting predictions. On the landscape two ingredients are needed for a “bottom-up” prediction: an edge that allows environmental selection, and an assumption that the a priori probability distribution is pushing parameters towards this edge. Predictions follow, quite literally, from living on the edge. Thus inventing models is replaced by finding edges and inventing probability distributions. There are two difficulties with this approach: relevant edges are hard to come by, and even if environmental selection is occurring at an edge, we can only discover it if the probability distribution happens to be favorable.

If the LHC discovers a light Higgs boson in our predicted range, and no sign of any physics beyond the SM, then a precise numerical test of environmental selection could follow from further developments in both theory and experiment. This will require a reduction in the experimental error bars of the QCD coupling and the top quark mass, and improved accuracy of calculations of both RG scaling and extracting pole masses from running couplings. In the

case that the phase boundary is determined by thermal fluctuations at high temperatures, a refined calculation of the temperature dependent effective potential will be needed, in particular including the effects of Higgs quanta in the thermal bath.

We conclude by addressing those who are sceptical of physics arguments from environmental selection. We have shown how precise predictions for the Higgs and top masses arise from assumptions about the landscape. If these precise predictions are found to be false, then our theoretical construct will be experimentally disproved. If they are found to be correct, then the SM is indeed on the edge of electroweak vacuum instability. It would then be up to you to find an alternative, more convincing theoretical framework to explain this fact. In this situation, we suspect that effort will be focussed on extracting further predictions from the landscape, and on understanding how the landscape might arise from string theory.

Acknowledgments

We thank A. Strumia for communications. This work was supported in part by the Director, Office of Science, Office of High Energy and Nuclear Physics, of the US Department of Energy under Contract DE-AC03-76SF00098, in part by the National Science Foundation under grant PHY-04-57315 and in part by Miller Institute for Basic Research in Science. LH and TW thank the Aspen Center for Physics where this work was completed.

A A Little More about The Thermal Effective Potential

At the 1-loop level, the effective potential in a thermal bath $V_{\text{tot}}(H)$ can be split into a sum of the effective potential at $T = 0$ and a thermal 1-loop contribution, $V_{TH}(H; T)$. The thermal contribution is given by [22, 23, 18, 24]

$$V_{TH}(H; T) = \frac{T^4}{2\pi^2} \left(6J_B \left(\frac{g_L H}{2 T} \right) + 3J_B \left(\frac{\sqrt{g_L^2 + g_Y^2} H}{2 T} \right) - 12J_F \left(\frac{h H}{\sqrt{2} T} \right) \right), \quad (56)$$

where

$$J_B(y) = \int_0^\infty dx x^2 \ln \left(1 - e^{-\sqrt{x^2 + y^2}} \right), \quad (57)$$

$$J_F(y) = \int_0^\infty dx x^2 \ln \left(1 + e^{-\sqrt{x^2 + y^2}} \right). \quad (58)$$

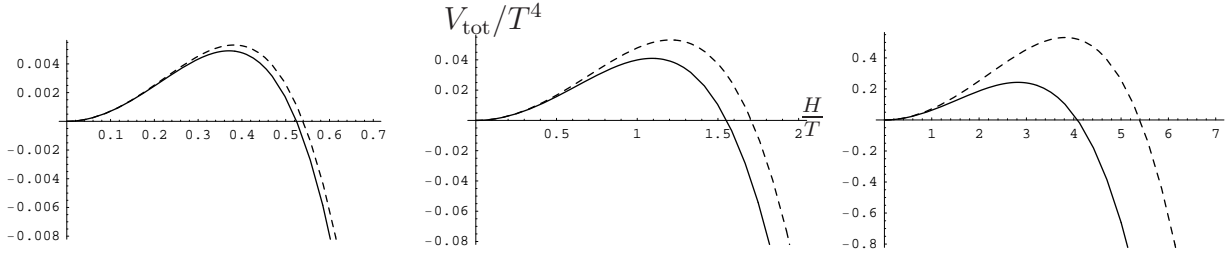


Figure 9: Effective potential in the thermal bath $V_{\text{tot}}(H)$ for different values of λ , (from left) -1 , -0.1 and -0.01 . The potential with (56) is drawn by solid lines, and with its approximation (33) by dashed lines. Using $g_L = 0.570$, $g_Y = 0.402$ and $h = 0.547$, we find $g_{\text{eff}} \simeq 0.382$ and $g_{\text{eff}}^4 \sim 0.02$ for $T = 10^{10}$ GeV and $m_H = 120$ GeV.

Here, only contributions of loops of W-bosons, Z-bosons and top quarks are taken into account, and not of the Higgs field itself. For Higgs field values much less than the temperature, this thermal contribution to the effective potential is approximated by a free energy piece plus quadratic term. On the other hand, for $T \ll H$, $V_{TH}(H; T)$ in (56) is exponentially small.

For a negative Higgs quartic potential with large $|\lambda(T)|$, the potential barrier for the vacuum transition is at a small field value of H . Hence, the overall shape of the potential is almost properly obtained even if the thermal contribution is approximated by the quadratic term (see Figure 9a). On the other hand, for a small $|\lambda(T)|$, the potential barrier is outside the range where the high-temperature expansion is valid, and V_{tot} calculated using the quadratic approximation for the thermal contribution (33) is quite different from the right shape of the potential (see Figure 9c). The quadratic approximation $V_{TH}^{(2)}(H; T)$ in (33) continues to grow for large H , but the true form of $V_{TH}(H; T)$ levels off for $H \gg T$. Thus, the potential using the quadratic approximation tends to overestimate the height and width of the potential barrier of the vacuum transition for small $|\lambda|$. From Figure 9 a–c, the quadratic approximation of the thermal potential is good for $|\lambda| \sim 1 \gg g_{\text{eff}}^4 \sim 10^{-2}$, but clearly not for $|\lambda| \sim 10^{-2}$.

Since the quadratic approximation of the thermal potential $V_{TH}(H; T)$ overestimates the height and width of the potential barrier for small $|\lambda|$, the bounce action $S_3/T \simeq 6.015 \pi g_{\text{eff}}/|\lambda|$ based on the approximation is also an overestimation. Figure 10a shows the bounce action calculated numerically with the full form of the potential $V_{TH}(H; T)$ in (56) and with $V_{TH}^{(2)}(H; T)$ in (33). Figure 10b shows the ratio between them. As expected from the difference in the shape of the potential in Figure 9, the bounce action is overestimated in (35)—by 20–30% from Figure 10b for $|\lambda| \sim 0.02$ – 0.04 , the range of practical interest. Thus, if the landscape prediction of the Higgs boson mass were calculated upon the quadratic approximation, $\lambda_c(T)$ would have been

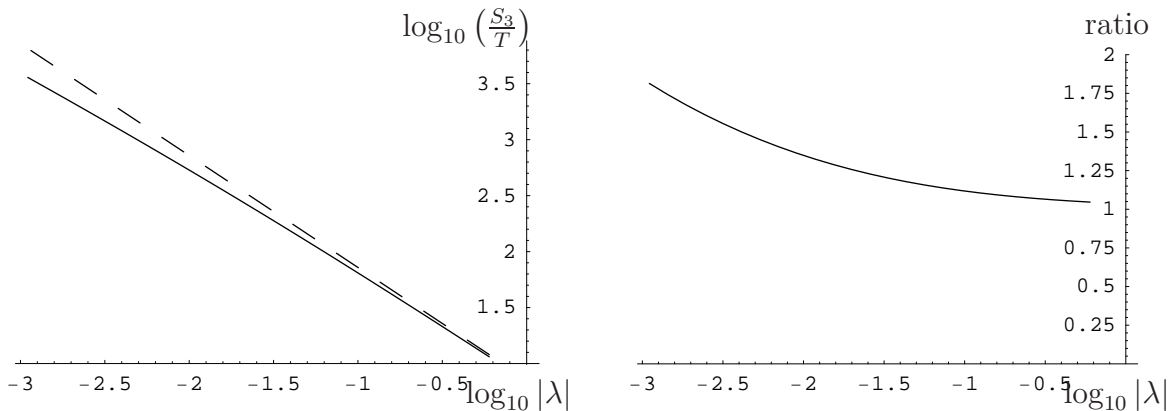


Figure 10: The bounce action S_3/T with (dashed) and without (solid) quadratic approximation of the thermal potential.

20–30% smaller, corresponding to λ at the weak scale being 10% smaller, and the prediction for \bar{m}_H being 5% lower. It is not appropriate to use the quadratic approximation to calculate $\lambda_c(T)$ and to obtain a precise landscape prediction. All the calculations in section 4 use the potential (56), and the bounce solution and action were obtained and calculated numerically. We used $m_H = 120$ GeV as the boundary condition of the 2-loop RG equations in order to calculate g_Y , g_L and h at high energy scale used in (56), but there is no impact on the result shown in Figure 7, even if $m_H = 130$ GeV is used instead.

On the other hand, Figure 10a also tells us that (35) captures the qualitative aspects very well; the numerically calculated bounce action (solid line) behaves almost the same way as (35). Thus, the expression (35) as an approximation of the bounce action is still quite useful when thinking of qualitative issues.

The biggest problem with the treatment of the thermal potential so far is that Higgs loops have not been included in (56).¹⁹ The contribution to g_{eff}^2 has also been omitted; it would have been

$$g_{\text{eff}}^2 = \frac{1}{12} \left(\frac{3}{4} g_Y^2 + \frac{9}{4} g_L^2 + 3h^2 + 6\lambda \right). \quad (59)$$

It is technically quite involved to incorporate the Higgs loop contribution to the thermal potential, when the high-temperature expansion is no longer valid. This is beyond the scope of this paper. Instead, let us try to get a feeling for the size of the possible effects of the Higgs loop contribution, using expressions in the quadratic approximation, which seems to be qualitatively

¹⁹The contribution from bottom quark loops is irrelevant to the calculation of the bounce action so long as $h_b^4 \ll |\lambda|$.

valid. The 6λ contribution in g_{eff}^2 leads to a 5% change in g_{eff} for $|\lambda| = 0.03$. A shift in $\lambda_c(T)$ of roughly 5% maintains the value of the bounce action (35), corresponding to a 2% change in the Higgs quartic coupling at the electroweak scale, and 1% change in the Higgs mass prediction. This estimate, however, heavily relies on the high-temperature expansion, and thus may not be particularly accurate.

References

- [1] N. Cabibbo, L. Maiani, G. Parisi and R. Petronzio, Nucl. Phys. B **158**, 295 (1979); P. Q. Hung, Phys. Rev. Lett. **42**, 873 (1979); M. Lindner, Z. Phys. C **31**, 295 (1986); M. Lindner, M. Sher and H. W. Zaglauer, Phys. Lett. B **228**, 139 (1989).
- [2] M. Sher, Phys. Rept. **179**, 273 (1989); B. Schrempp and M. Wimmer, Prog. Part. Nucl. Phys. **37**, 1 (1996) [arXiv:hep-ph/9606386].
- [3] M. Sher, Phys. Lett. B **317**, 159 (1993) [Addendum-ibid. B **331**, 448 (1994)] [arXiv:hep-ph/9307342]; G. Altarelli and G. Isidori, Phys. Lett. B **337**, 141 (1994); J. A. Casas, J. R. Espinosa and M. Quiros, Phys. Lett. B **342**, 171 (1995) [arXiv:hep-ph/9409458]; T. Hambye and K. Riesselmann, Phys. Rev. D **55**, 7255 (1997) [arXiv:hep-ph/9610272].
- [4] G. Isidori, G. Ridolfi and A. Strumia, Nucl. Phys. B **609**, 387 (2001) [arXiv:hep-ph/0104016].
- [5] The LEP Collaborations, the LEP Electroweak Working Group, and the SLD Electroweak and Heavy Flavour Groups, arXiv:hep-ex/0509008, as updated on <http://www.cern.ch/LEPEWWG>
- [6] R. Barbieri and A. Strumia, arXiv:hep-ph/0007265.
- [7] F. Hoyle, “*Galaxies, nuclei and quasars*,” Heinemann, London, 1965, p 146 and p 159.
- [8] V. Agrawal, S. M. Barr, J. F. Donoghue and D. Seckel, Phys. Rev. D **57**, 5480 (1998) [arXiv:hep-ph/9707380].
- [9] S. Weinberg, Phys. Rev. Lett. **59**, 2607 (1987); H. Martel, P. R. Shapiro and S. Weinberg, Astrophys. J. **492**, 29 (1998) [arXiv:astro-ph/9701099].
- [10] R. Bousso and J. Polchinski, JHEP **0006**, 006 (2000) [arXiv:hep-th/0004134]; M. R. Douglas, JHEP **0305**, 046 (2003) [arXiv:hep-th/0303194]; S. Ashok and M. R. Douglas, JHEP **0401**, 060 (2004) [arXiv:hep-th/0307049]; T. Banks, M. Dine and E. Gorbatov, JHEP

- 0408**, 058 (2004) [arXiv:hep-th/0309170]; F. Denef and M. R. Douglas, JHEP **0405**, 072 (2004) [arXiv:hep-th/0404116]; A. Giriyavets, S. Kachru and P. K. Tripathy, JHEP **0408**, 002 (2004) [arXiv:hep-th/0404243]; O. DeWolfe, A. Giriyavets, S. Kachru and W. Taylor, JHEP **0502**, 037 (2005) [arXiv:hep-th/0411061].
- [11] C. D. Froggatt and H. B. Nielsen, Phys. Lett. B **368**, 96 (1996) [arXiv:hep-ph/9511371].
- [12] C. D. Froggatt, H. B. Nielsen and Y. Takanishi, Phys. Rev. D **64**, 113014 (2001) [arXiv:hep-ph/0104161];
- [13] K. M. Lee and E. J. Weinberg, Nucl. Phys. B **267**, 181 (1986).
- [14] A. H. Guth and E. J. Weinberg, Phys. Rev. D **23**, 876 (1981); A. D. Linde, Nucl. Phys. B **216**, 421 (1983) [Erratum-ibid. B **223**, 544 (1983)].
- [15] W.-M. Yao et al., J. Phys. G **33**, 1 (2006) [Particle Data Group].
- [16] C. Ford, D. R. T. Jones, P. W. Stephenson and M. B. Einhorn, Nucl. Phys. B **395**, 17 (1993) [arXiv:hep-lat/9210033].
- [17] A. Sirlin and R. Zucchini, Nucl. Phys. B **266**, 389 (1986).
- [18] M. Sher in [3].
- [19] R. Hempfling and B. A. Kniehl, Phys. Rev. D **51**, 1386 (1995) [arXiv:hep-ph/9408313].
- [20] T. Hambye and K. Riesselmann in [3].
- [21] N. Arkani-Hamed, S. Dimopoulos and S. Kachru, arXiv:hep-th/0501082.
- [22] G. W. Anderson, Phys. Lett. B **243**, 265 (1990).
- [23] P. Arnold and S. Vokos, Phys. Rev. D **44**, 3620 (1991).
- [24] J. R. Espinosa and M. Quiros, Phys. Lett. B **353**, 257 (1995) [arXiv:hep-ph/9504241].
- [25] E. Kolb, M. Turner, *“The Early Universe,”* Addison–Wesley, 1990.
- [26] R. Harnik, G. D. Kribs and G. Perez, arXiv:hep-ph/0604027.
- [27] J. F. Donoghue, K. Dutta and A. Ross, Phys. Rev. D **73**, 113002 (2006) [arXiv:hep-ph/0511219].
- [28] L. J. Hall, H. Murayama and N. Weiner, Phys. Rev. Lett. **84**, 2572 (2000) [arXiv:hep-ph/9911341].
- [29] W. Buchmuller, P. Di Bari and M. Plumacher, Annals Phys. **315**, 305 (2005) [arXiv:hep-ph/0401240]; W. Buchmuller, R. D. Peccei and T. Yanagida, Ann. Rev. Nucl. Part. Sci. **55**, 311 (2005) [arXiv:hep-ph/0502169].

- [30] M. Tegmark and M. J. Rees, *Astrophys. J.* **499**, 526 (1998) [arXiv:astro-ph/9709058]; M. Tegmark, A. Aguirre, M. Rees and F. Wilczek, *Phys. Rev. D* **73**, 023505 (2006) [arXiv:astro-ph/0511774].
- [31] P.C.W Davies, *Journal of Physics* **A5** 1296 (1972); L. Okamoto and C. Pask *Ann. Phys.* **68** 18 (1971); J. Barrow and F. Tipler, *The Anthropic Cosmological Principle*, Clarendon Press, Oxford, 1986.
- [32] A. Aguirre, arXiv:astro-ph/0506519.
- [33] A. Linde, *Phys. Lett. B*201, 437 (1988); F. Wilczek, hep-ph/0408167.